Schweizerische Eidgenossenschaft
Confédération suisse
Confederazione Svizzera
Confederaziun svizra

Federal Department of the Environment, Transport, Energy and Communications DETEC

Swiss Federal Office of Energy SFOE
Energy Research and Cleantech

Final report

RESTART (VOLTA)

Robust and Scalable Titanate Anodes for Industrial SOC Applications

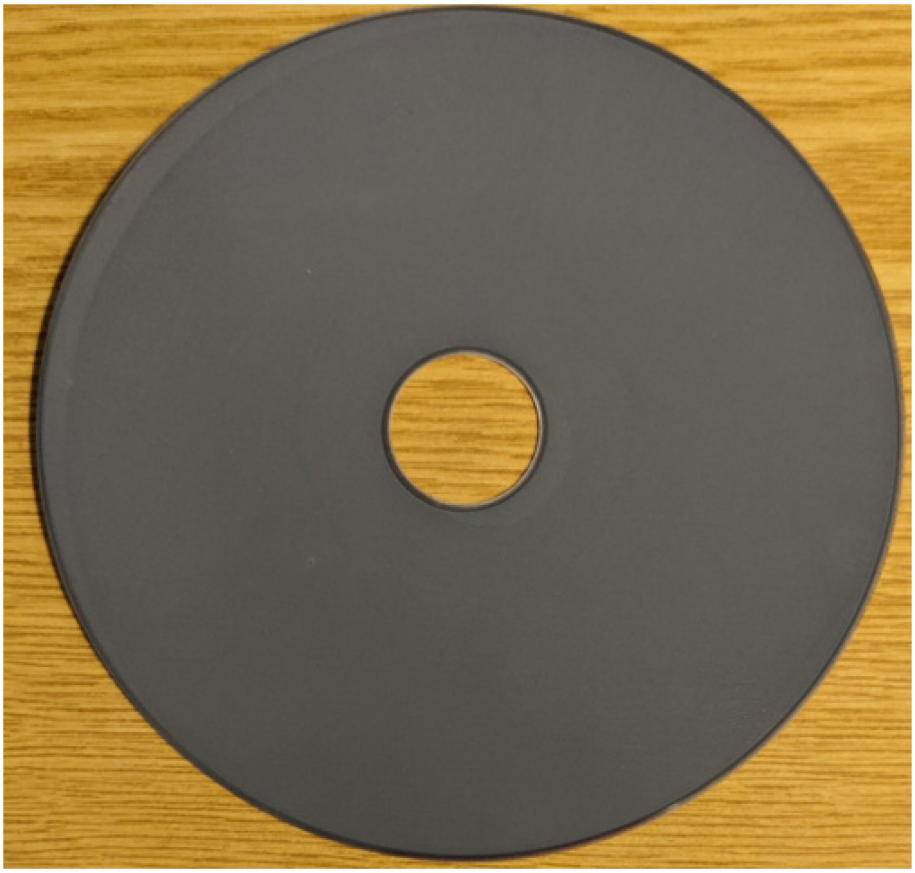

Source: ©Hexis

Date: 31st January 2023

Location: Bern

Publisher:
Swiss Federal Office of Energy SFOE
Energy Research and Cleantech
CH-3003 Bern
www.bfe.admin.ch

Agent:
HEXIS AG
Zum Park 5
CH-8404 Winterthur
www.hexis.com

Authors:
Dr Holger Bausinger, Hexis AG, holger.bausinger@hexis.com
Dr Andre Heel, OST, andre.heel@ost.ch
Dr Lorenz Holzer, ZHAW, holz@zhaw.ch
Dr. Philip Marmet, ZHAW, mame@zhaw.ch

SFOE project coordinators:
Dr. Stefan Oberholzer, Stefan.oberholzer@bfe.admin.ch

SFOE contract number: SI/501792-01

Zusammenfassung

Das RESTART Projekt ist als Re-Fokus aus dem VOLTA Projekt abgeleitet. Dabei wurde ein Schwerpunkt auf die Zusammensetzung der Anodenfunktionsschicht gelegt, die mittels Simulation und Modellierung sowie intensiver Mikrostrukturanalysen (ZHAW) optimiert wird. Eine weitere zentrale Rolle spielt die produktionsnahe Herstellbarkeit von Edelmetall-imprägnierten Anodenbackbone-Schichten. Eine industrielle Umsetzung wird angestrebt (Hexis AG). Auf der Materialebene werden Leistungsoptimierungen einzelner Komponenten vorgenommen. So soll z.B. die Perowskit-Komponente bezüglich ihrer elektrischen Leitfähigkeit bei Betriebsbedingungen verbessert werden (OST).

Summary

The RESTART project is derived as a re-focus from the VOLTA project. A focus was placed on the composition of the anode functional layer, which is optimized by means of simulation and modelling as well as intensive microstructure analyses (ZHAW). Another central role is played by the near-production manufacturability of precious metal-impregnated anode backbone layers. Industrial implementation is being sought (Hexis AG). At the material level, the performance of individual components is being optimized. For example, the perovskite component is to be improved with regard to its electrical conductivity under operating conditions (OST).

Résumé

Le projet RESTART est dérivé du projet VOLTA. L'accent a été mis sur la composition de la couche fonctionnelle de l'anode, qui est optimisée au moyen de la simulation et de la modélisation ainsi que d'analyses intensives de la microstructure (ZHAW). Un autre rôle central est joué par la possibilité de fabriquer en quasi-production des couches dorsales d'anode imprégnées de métaux précieux. La mise en œuvre industrielle est recherchée (Hexis AG). Au niveau des matériaux, les performances des composants individuels sont optimisées. Par exemple, le composant pérovskite doit être amélioré en ce qui concerne sa conductivité électrique dans les conditions d'exploitation (OST).

Contents

Abbreviations

SFOE	Swiss Federal Office of Energy
CHP	Combined heat and power unit
SOFC	Solid oxide fuel cell
SOEC	Solid Oxide Electrolysis Cell
SOC	Solid oxide cell
CGO	Cerium Gadolinium Oxide
ASR	Area specific resistance
HOR	Hydrogen oxidation reaction
ECM	Equivalent circuit model
DRT	Distributed relaxation time
DOD	Drop on Demand
OCV	Open Circuit Voltage
LSCT	Lanthanum Strontium Calcium Titanate
L-TPB	Length of triple phase boundary
LSCF	Lanthanum Strontium Cobalt Ferrum (Iron)

1 Introduction

1.1 Background information and current situation

Fuel cell systems enable the simultaneous provision of electricity and heat in buildings, even in power classes that enable the supply of single-family homes (micro-CHP). Here, higher electrical efficiencies than in conventional comparison technologies (internal combustion engine, Stirling engine, steam engine, etc.) are possible and have been demonstrated in products.

In 2013, HEXIS was one of the first companies worldwide to launch a fuel cell heating system, the Galileo 1000 N. Galileo was manufactured more than 300 times. Due to limited component availability, it is no longer manufactured. Approximately 150 devices are still and will continue to be in operation and are managed by HEXIS.

The project, specifically, focuses on the development of a novel, industrially scalable, electrolyte-supported fuel cell and its development to prototype maturity. The aim of the project is to systematically investigate robust titanate materials as catalytically active anode current collectors and implement them into a proven electrolyte-supported fuel cell microstructure. This new anode microstructure should be also compatible with Solid Oxide Electrolysis applications and, in contrast to current cell technology, significantly more tolerant to overload and fuel contamination. Successful engineering implementation is achieved by combining latest findings from materials science with modern methods of materials modelling and microstructure analysis. This approach enables to define appropriate design recommendations for material-microstructure-performance correlations and to realize them for practical application.

One of the main goals of past projects was to significantly reduce CHP manufacturing costs and increase operational robustness. In particular, the balance-of-plant (that is, the "cold" components such as fans, inverters, heat exchangers, gas valves, etc.) were changed or new suppliers established. In addition, the design has been significantly changed in the stack module and associated insulation in order to significantly reduce the manufacturing costs there as well. Overall, the manufacturing costs could thus be lowered by about 50% compared to Galileo. The fuel cell stack remains unchanged compared to Galileo.

In the da Vinci project, steam reforming is being established in the device in order to further increase the electrical efficiency. In the Fermi project, a ferritic interconnector including manufacturing process was developed, which can be mass-produced and allows a significant reduction in the manufacturing costs of the stack, as well as a significant reduction in aging and thus a significant increase in service life.

1.2 Purpose of the project

The characteristic properties of Hexis SOFC are in principle very good. In addition to a high energy efficiency, the stacks have a high long-term stability and thus a long service life (>40'000 hours).

a) This applies analogously to the state-of-the-art anode, which, however, still has considerable potential for optimization in the following areas due to the wide range of tasks and requirements:

- Damage to the anode during initial heating
- Damage to the anode in case of overload
- Sulphur intolerance

The improvement of these properties is described in chapter 2.3 Project Goals.

b) In addition, future requirements for an anode/fuel gas electrode, especially in new products to be developed, have not been investigated or not sufficiently investigated so far. Especially in combination with h2e and mPower, it is planned not to be limited to natural gas-based SOFC applications. These include:

- Function as fuel gas electrode in electrolysis mode (SOEC) or reversible SOC (r-SoC)
- Compatibility with biogas as a fuel gas, for use in agricultural SOFC electricity generators

c) Experimental laboratory tests have identified a new material system that can at least partially meet the requirements. It has been shown (proof-of-concept) that anodes containing LSCT (a titanate material) impregnated with a catalytically active metal have a particular stability or robustness against the disturbances described in a). The results so far are promising, but further optimization and investigations are still necessary to reach maturity for series production. In particular, the reasons for the improved performance are not yet sufficiently understood. Some of the requirements have not yet been investigated (SOEC, biogas) and cost optimization has not yet taken place. In addition, the technical feasibility on an industrial scale has yet to be established.

1.3 Objectives

Based on the above motivation, the following objectives for the anode system result in brief:

- Stability/robustness during initial heating in SOFC operation:
  No damages or degradation should occur due to faults in the initial heating process (less than 1 mΩcm2/1000h)
- Stability/robustness in overload situations in SOFC operation:
  No damages or additional degradation should occur due to special situations in the real operating mode (i.e. power outages, gas failure)
- Tolerance to sulphur contamination in fuel gas, SOFC operation:
  The anodes should be able to withstand sulphur fluctuations in the gas network as well as the short-term failure of the desulphuriser (up to 24h).
- Capability as fuel gas electrode in SOEC operation:
  High electrochemical performance/hydrogen output and long-term stability (>40’000 h) are required in SOEC operation
- Capability for utilization of biogas:
  The use of biogas should be possible for SOFC modules, i.e. in agricultural sectors without access to natural gas. The lifetime of such systems is required to exceed 40’000 h.
- Basic understanding for anode processes regarding the new material system:
  This understanding enables the achievement of the projected goals and the further optimization of the properties in the future
- Construction and optimization of equipment for scalable cell production, in particular impregnation methods for the catalytically active metal component:
  A pilot equipment for cell impregnation is to be installed within the project to be able to conduct all necessary test series for anode development as well as the elaboration of all production parameters to build up a stable pilot production process for at least 20’000 cells/year.
- Development of key know-how at the Winterthur site (materials and production expertise):
  Establishment of a well-trained production and development team to make the site one of the leading SOC production centers in Europe

- Cost optimization of the materials used and the manufacturing processes:
  The right choice of materials and production processes should contribute to a competitive cost structure, especially with regard to series production.

To achieve these objectives, a multi-level strategy with the following work packages is envisaged:

- Microstructural analysis, modelling and optimization (WP2, WP5)
- Development of a ceramic backbone and optimization of composition and properties like the electrical conductivity (WP3)
- Development of production process, the built up of pilot equipment, cell and stack testing, Upscaling and quality assurance for serial production of cells (WP1, WP4)
- Optimization of catalytic materials (WP6)

2 Procedures and methodology

The RESTART project is well embedded into the Hexis project environment. Externally, the project benefits from projects in the area of stack and systems development (i.e. SFOE funded DaVinci, EU supported PACE project), also RESTART benefits of projects focusing on the cell development like SERAN (SFOE), SCOTAS (EU), NewSOC (EU) but also Fermi (SFOE).

Looking forward - the RESTART project will also enable new developments and therefore also future projects in areas like stack development, renewable fuels and, also, solid oxide electrolysis operation. Due to the versatility of the targeted anode materials the outcome of the RESTART project will widen the HEXIS' technology portfolio and therefore offer new areas of activities for Hexis beyond the SOFC based CHP application currently pursued.

3 Activities and results

3.1 Scalable Catalyst Impregnation (WP1: Hexis, iPrint)

3.1.1 Overview of workplan and deliverables

In WP1, the catalyst (i.e. Rhodium salt solutions) shall be scaled from a laboratory level method – that is needed to prepare samples for button cell and short stack testing in WP4 – to an industrial process for efficient, reliable and cost effective production of solid oxide cells. As one of the most interesting catalyst impregnation process, inkjet printing was chosen because the catalyst solution can be applied directly and in a precise manner on top of the anode backbone layer of a SOC, which gives the possibility to dose exactly the required amount of catalyst without scrap. For laboratory use, a conventional desktop printer was successfully applied within a master thesis at Hexis. For the implementation of an industrial scale inkjet process, a feasibility study was carried out with iPrint (Applied research institute for digital printing, University of Applied Sciences and Arts Western Switzerland, Fribourg). A commercially available printhead was found and cell prototypes were produced and successfully tested.

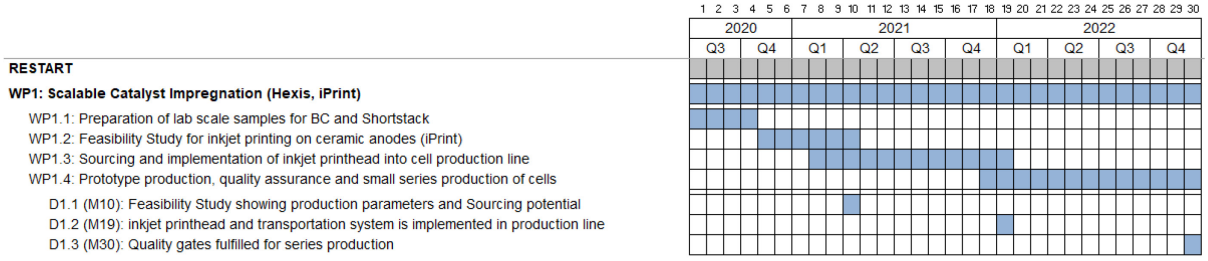

Figure 1: Gantt-chart and deliverables for work package 1 (Scalable Catalyst Impregnation)

3.1.2 Feasibility Study for inkjet printing on ceramic anodes (iPrint)

A feasibility study is being elaborated by iPrint (Applied research institute for digital printing, University of Applied Sciences and Arts Western Switzerland, Fribourg).

In the last report we examined the rheological properties and the surface tensions of the catalyst inks, presented the most promising ink composition, and tested successfully the application of Rhodium acetate instead of Rhodium nitrate.

Printhead selection

The possible printheads were discussed and it was decided that the compatibility test will be performed on the EPSON I3200 printhead. A compatibility test kit was ordered from Epson as most promising print head manufacturer for our purposes.

Epson Compatibility Test

The result of the test was that a corresponding Epson print head shows a small incompatibility towards the as-formulated ink. Moreover, it is believed that by increasing the water content or decreasing the salt concentration for the ink formulation, the latter one will become more compatible with the printhead.

In conclusion, iPrint plans to use an Epson printhead for the upcoming while starting to investigate the printhead jetting and printing performance over time and thus evaluate a time of life of the printhead.

Full cells inkjetted by the Epson printhead with catalyst solution

To complete the feasibility study, 15 full cells prepared by Hexis (anode backbone: double-layered 50% CGO / 50% LSCT; cathode: standard Hexis layers) were ink jetted with 4% Rh acetate solution (30% IPA / 70% H_2O) on a laboratory scale x/y table, equipped with an Epson I3200 printhead.

Different Rh acetate loadings could be realised by altering the number of pulses per notch (4, 5, and 6 Pulses). The Rh acetate depositions could each be calculated by measuring the cell weight before and after inkjetting and subsequent infrared drying of the cell surface. One cell of the series is shown in Figure 2.

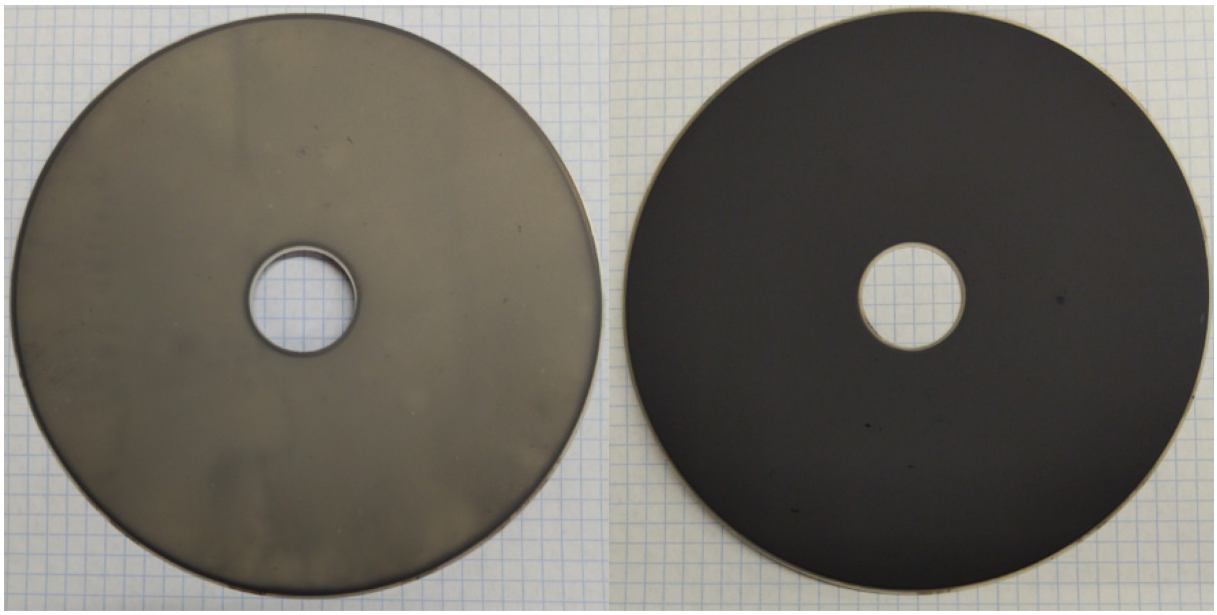

Figure 2: Rh acetate inkjet impregnated anode (left) and untreated cathode (right) after calcination at 500°C

The printing results are:

- The full cell with 120m in diameter could be printed in four Lanes, with only slightly overlapping of the lanes. For the future, it is possible to print the whole cell in one single lane by using a double printhead with 2x 60mm width (also an EPSON product: S3200).
- A homogeneous impregnation distribution could be achieved, which can be seen optically after calcination at 500°C (see Figure 2).
- The Rh acetate ink is expected to penetrate through the whole anode layer thickness, because there was a complete wetting of the anode backbone. This expectation has to be confirmed by a Shortstack test.

Shortstack testing of the electrochemical performance

A shortstack test was performed with the following cells:

- #2 and #6: 5 Pulses, 0.0057 g Rh acetate loading
- #7: 4 Pulses, 0.0047 g Rh acetate loading
- #8: 6 Pulses, 0.0070 g Rh acetate loading
- Ref: reference Hexis Standard cell

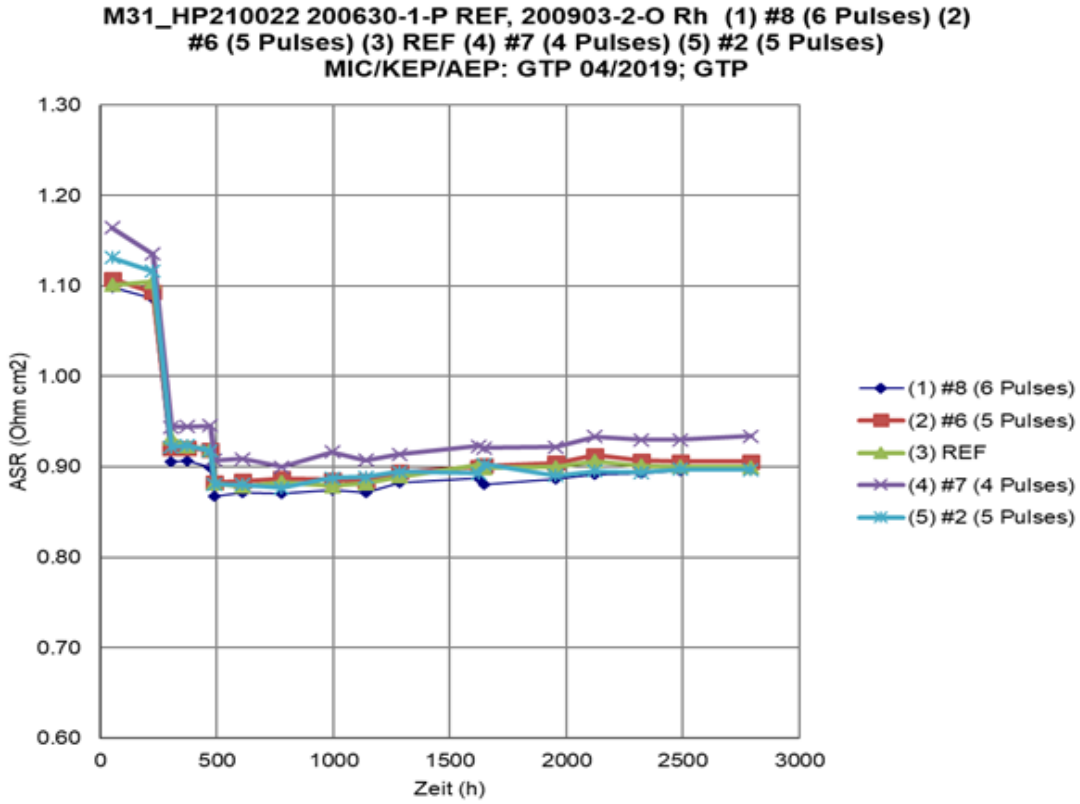

Figure 3: Shortstack test of 4 Rh acetate inkjet impregnated cells with a Hexis standard cell as reference

The result is shown in Figure 3. Within the first 500h, some adjustments were made to compensate a technical issue with the air supply at the cathode. What is way more interesting: the five cells show almost the same electrochemical performance, which is, comparing with figures 3 and 4 of the December 2021 report, a strong indication that Rh penetrates deep into the anode backbone, leading to a fully functionable anode electrode.

Before shutting down the test rig, an overload test was performed on this stack. The current was increased from 25 A to 35 A. This overload resulted in a fuel gas utilization of more than 100% leading to a gas depletion on the anode side of the cells. Three cycles were applied, each taking several hours, with a recovery phase overnight back to 25 A. The result is shown in Figure 4.

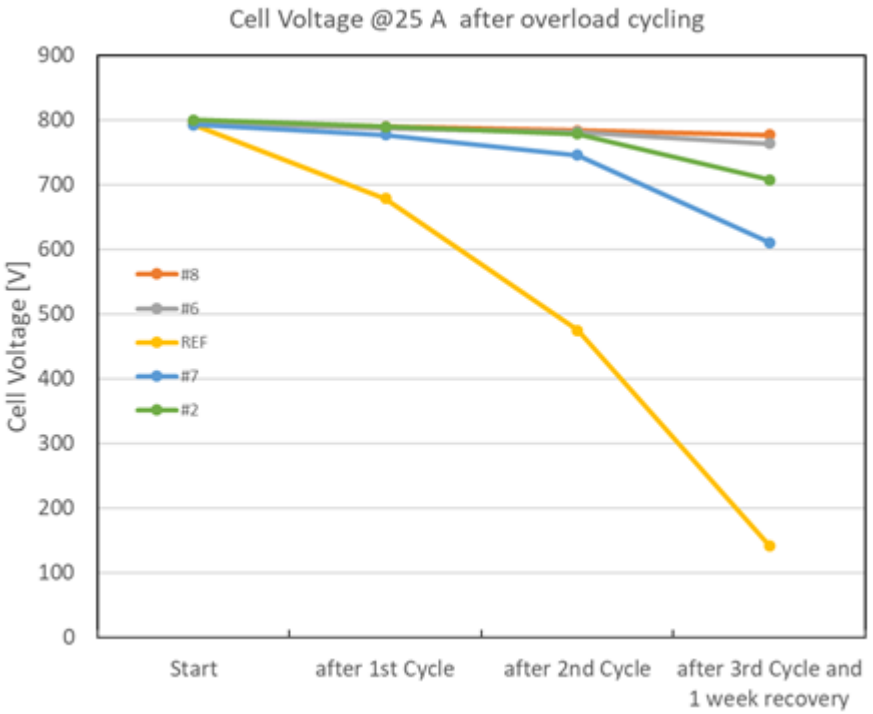

Figure 4: Overload testing of the Shortstack test shown in Figure 3.

The cell voltage of the Hexis standard cell is significantly reduced after 3 cycles, showing severe damage in contrast to the Rh impregnated titanate anode cells. The damage of the Rh cells seems to be slightly dependent on the Rh content. The loss in cell voltage as a measure of the damage or degradation is roughly increasing with decreasing Rh content. With future experiments on Rh ink jetted full cells it is planned to examine the optimised Rh content in terms of performance, degradation, and overload robustness.

The key result of the study is that the impregnation method with Rh acetate using a professional Epson printhead is feasible for application in a SOFC stack.

To further confirm these results on a system scale, a series of 100 full cells were produced with the parameters of 5 pulses per nozzle (comparable to cells #2 and #6 in Figure 3). At least one full stack has been assembled and a system test was started at the end of June 2022. The focus of the investigation lies here the long-term degradation observations. A second full stack, comprising a mixture of HEXIS standard cells and the Rh titanate cells of this 100-series, will be assembled and run on a system scale later this year, where the focus lies on the thermoredox cycling, overload conditions, and simulated incidents to observe the robustness of the both cell types.

3.1.3 Sourcing and implementation of inkjet printhead into cell production line (iPrint, Hexis)

iPrint and Hexis has started in March 2022 a project application at Innosuisse for the funding of the development of an industrial process. At the time of writing, the funding is granted for a two-years period. We saw that in the frame of the RESTART project it is not possible to establish a fully equipped production facility. This is simultaneously due to overall time delays (Covid-19) and challenging business conditions at Hexis (market entry delayed, lack of ressources etc.). The work package 1.3 will therefore not be started in this RESTART framework.

3.2 Modelling and optimization of anode architecture and microstructure (WP2: ICP ZHAW)

3.2.1 Overview of workplan and deliverables

The aim of WP 2 is to promote the development of a new composite CGO-titanate anode with catalyst nanoparticles based on a modelling-approach. In this approach we use digital materials design (DMD), which combines various methodologies for modelling and characterization. Thereby, the numerical electrode model provides a basic understanding of the involved processes and helps to interpret experimental results (e.g., EIS) in a reliable way. A systematic data-analysis of experimental EIS spectra and continuous literature study are also important tasks of WP 2. DMD-based optimization of the microstructure is also achieved with input from WP5 (quantitative microstructure analysis). Thereby, tomography and microstructure modelling are used to vary the microstructures in a realistic way, and to predict the corresponding properties. The DMD approach is thus a combination of all information and methods from experimental characterization of cell-performance, literature study, microstructure analysis and modelling. From a parametric DMD study, design guidelines for optimized anode and cell fabrication are formulated in an iterative process.

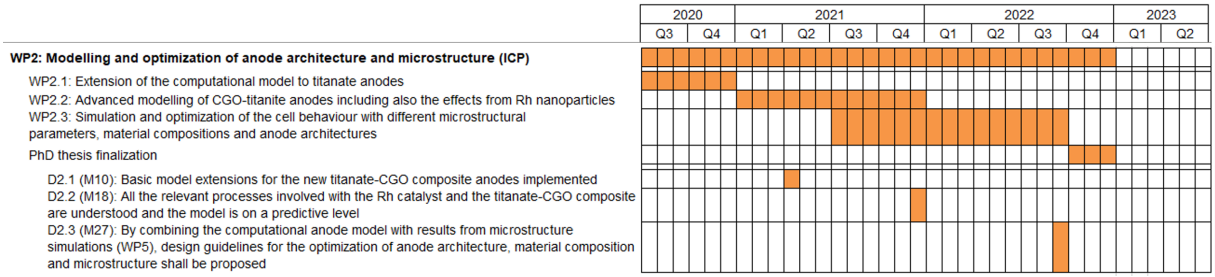

Figure 5: Gantt-chart and deliverables for work package 2 (Modelling and optimization)

3.2.2 Digital microstructure variation of the LSCT-CGO electrodes

In the previous reports, the development and application of Digital Materials Design (DMD) for the optimization of titanate-CGO anodes was presented. For this report period, design guidelines for the titanate CGO anodes shall be reported (deliverable D2.3, milestone M27), which were deduced by connecting all information from the experimental work, literature study and the results from the DMD-optimization. The following section thus represents a qualitative discussion of design guidelines for anode concepts with potentially higher initial performance and with improved long term stability.

Nickel-free electrodes are expected to show higher robustness against carbon coking, sulfur poisoning and redox-cycling [1] [2] and a higher mechanical stability [3]. A promising approach is to use perovskite-CGO ceramic composite anodes instead of the well-known Ni-YSZ or Ni-CGO cermets. However, perovskite-CGO anodes with high perovskite contents often show a worse initial performance, e.g., in comparison to Ni-CGO anodes. The initial anode ASR decreases with increasing CGO-contents, as demonstrated in this work (see previous reports) and in several studies in the literature (Sciazko et al. [3] and Burnat et al. [4]). For titanate-perovskite, a significant contribution to the HOR reaction is observed in this work for LSCT (La-Sr-Ca-Titanate) and by Burnat et al. [4] for LST (La-Sr-Titanate). However, this electrochemical perovskite contribution is not able to compensate the loss of electrochemical activity related to a reduction of the CGO-content, which is inevitably occurring when titanate-contents are increased. Moreover, the available perovskites do not reach the intrinsic ionic conductivity of CGO, which leads to a further reduction of the anode performance for increasing perovskite content. However, first tests indicating an improved degradation behaviour [3], [4], [5] and from this project are promising. Thus, perovskite-CGO electrodes have the potential to enable more robust, enduring and therewith more cost

effective SOFC/SOEC systems. But the initial performance needs to be improved. In the following, different possibilities for further improvement of the initial performance shall be stated by providing model-based design guidelines from DMD. In order to illustrate the basic concepts, a graphical illustration of the design guidelines is provided in Fig. 6. These concepts are briefly discussed below.

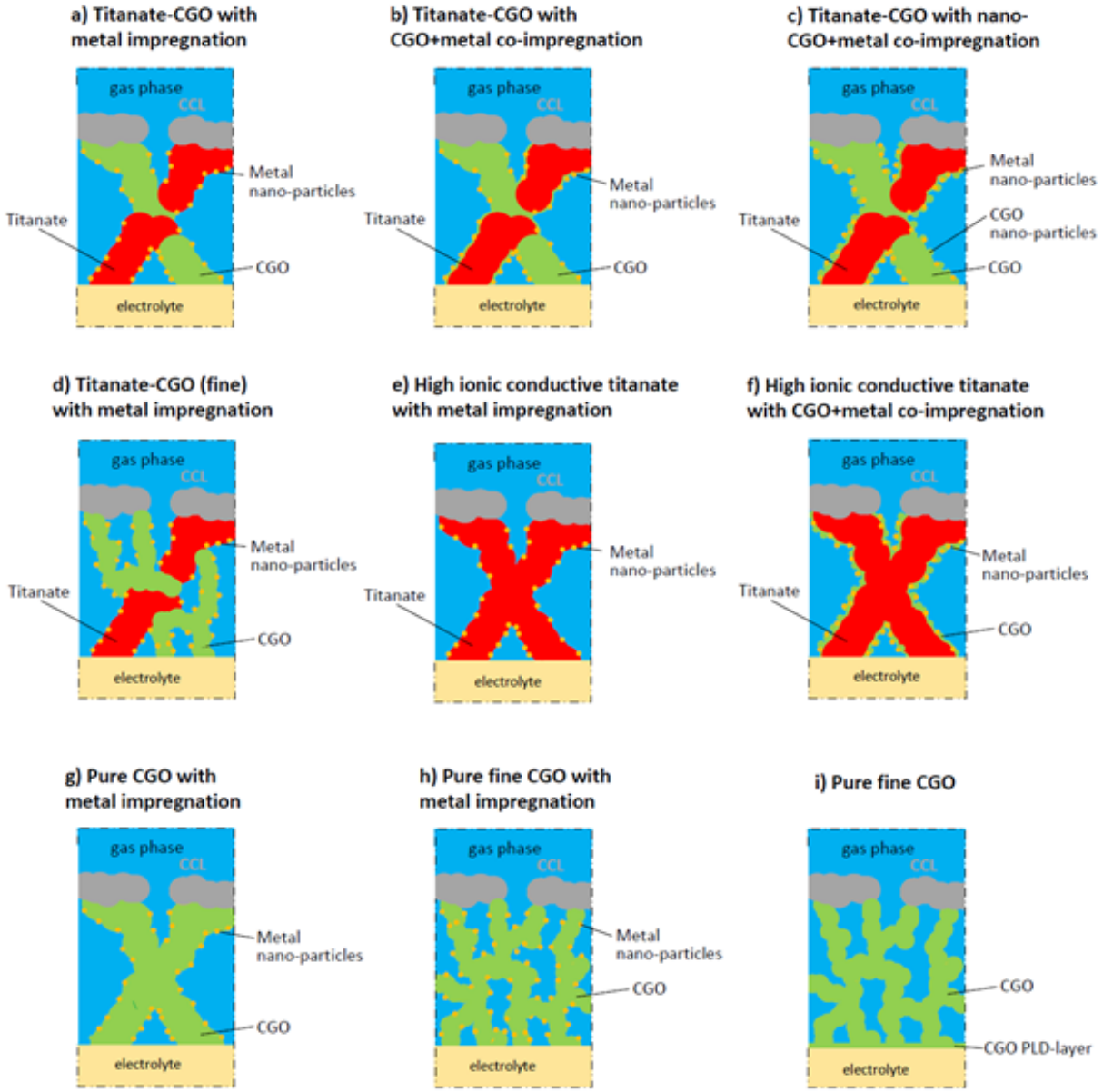

Figure 6: Graphical design guidelines for the optimization of Ni-free anodes.

First of all, the electrochemical activity of the anode is of major importance [2]. CGO generally provides a very good electrochemical activity. But the electrochemical activity of the anode is reduced when increasing the perovskite contents. This can be explained simply by the fact that the relative CGO-contents are decreasing (i.e., replaced by perovskite) and so is the highly active surface area of the CGO-pore interface. Moreover, it is well known that the Ni-surface in Ni-CGO anodes also acts as an electro-catalyst (e.g., Primdahl et al. [6]), which is no more present in the titanate-CGO anodes. Thus,

a possible approach to compensate the reduced electrochemical activity is to impregnate the electrode with a finely dispersed noble metal catalyst, as successfully demonstrated by several authors [7], [8], [9], [10]. This approach has already been applied in this project using Rh-impregnation. An additional or alternative approach to increase electrochemical activity is to increase the specific pore-CGO interface area with a finer microstructure or an additional CGO-impregnation (i.e., placing CGO nanoparticles on the perovskite-surface), as will be discussed later in this section.

Another aspect of major importance is the limited ionic conductivity of the titanates, which is associated with ohmic losses but also with a lower extension of the reaction zone and thus a higher HOR-reaction resistance. A possible optimization route, which addresses both, the improvement of the effective electrochemical activity and the effective ionic conductivity, is an appropriate design of the microstructure. First of all, a backbone that already includes CGO, provides a considerably higher ionic conductivity than a pure perovskite backbone. This approach together with the Rh-impregnation is illustrated in Fig. 6 a) and was already applied in this work for the LSCT-CGO anodes. For this specific design, the composition, the porosity and the AFL-thickness needs to be designed appropriately in order to optimize the trade-off between the reaction kinetics, charge and gas transport. The model-based optimization for this anode-concept was performed with our DMD approach, which includes a virtual structure variation based on real tomography data. Even though the best initial performance is predicted for a CGO content of 100 %, studies reported in literature suggest (Yoo et al. [11] and Sciazko et al. [3]) that a CGO-content of about 70 wt.% (corresponding to a volumetric CGO-content of approximately 62 vol.%) might be a good compromise between electrochemical performance (with high CGO-content) and structural stability (with low CGO-content). For this composition, a porosity of about 35 % is predicted to be appropriate based on our own simulations. Thus, the porosity of the actual LSCT-CGO electrodes around 30 % is already in a good range. A suitable AFL-thickness is predicted around L=23 µm. However, the dependency of the anode ASR on the AFL-thickness is very flat in the range between L=15-40 µm. Thus, when increasing the thickness of the current Hexis anode, which is around L=15 µm, it is not expected to provide a measurable improvement of performance. For the short-stack tests, two anode layers were printed, which corresponds to a total layer thickness of about L=20-30 µm, which is close to the simulated optimum. The virtual structure variations also shows that this anode material concept is quite robust and can tolerate some variations in the fabrication process (e.g., thickness, composition), and also in the operating conditions (e.g., gas flow rate, gas composition, current).

Moreover, a promising optimization route is the reduction of the characteristic particle size (i.e., bulges) of the solid phase, in order to increase the specific pore-CGO interface area and thus to improve the reaction kinetics, as illustrated for the green phase in Fig. 6 d). Due to an enhanced reaction kinetics, the extension of the reaction zone decreases and thus, the ionic transport (i.e. effective ionic composite conductivity) becomes less restrictive, because the ionic transport pathways from electrolyte to anode reaction site are shorter. Hence, this promising approach of reduced particle size is experimentally limited by the possibilities of processing and sintering of very fine powders, the stability of nano-sized structures at high temperatures and by the Knudsen effect, which drastically increases the gas transport resistance in very small pores. The latter point is less severe, as the higher electrochemical activity reduces the needed AFL-thickness and therewith limits the gas diffusion impedance. However, an option to circumvent both limitations would be an anode concept with a multi-scale structure that contains relatively large pores. This might be partially achieved by a relatively coarse LSCT-backbone, which is also included in the red-phase shown in Fig. 6 d). However, a relatively coarse LSCT-phase will need higher sinter temperatures than the fine-porous CGO-phase and thus, very different particle sizes of LSCT and CGO might not result in a stable structure. Another multi-scale approach would be to deposit small CGO nano-particles at the surface of a coarse backbone. In this anode concept, the current LSCT-CGO composite anodes could be used as a sintered backbone. CGO nano-particles or chemical precursors of CGO could then be introduced together with Rh by co-impregnation. A minimal effect would be that also the surface of LSCT is covered with CGO, which increases the available CGO-pore interface area, as illustrated with a thin green rim on the red phase in Fig. 6 b). A similar anode concept was already tested in a study by Futamura et al. [12] [13], where an anode with an LST-CGO backbone with 50:50 ratio by volume was additionally co-impregnated with CGO and a catalyst metal (Ni, Rh, Pd, or

Pt). The co-impregnated anodes (CGO+metal) thereby showed a considerably improved performance compared to anodes impregnated only with a metal. With a suitable impregnation technique, a considerably larger specific CGO-pore interface area can be achieved in a multi-scale anode concept consisting of a coarse backbone with CGO nano-particles. In this way, a microstructure with relatively large pores, but also with a large specific CGO-pore interface area could be achieved, due to the presence of CGO nano-particles at the surface of CGO and LSCT. This anode concept is illustrated in Fig. 6 c). The performance of an optimized structure according to this concept might even be sufficiently high without the addition of expensive noble metal catalysts [14], [15]. However, the feasibility of the fabrication of such a multi-scale structure and the stability of the CGO nano-particles at high operating temperatures would need to be verified experimentally. Promising approaches have been reported by Blennow et al. [16] (surfactant-assisted CGO-infiltration) and by Perillat-Merceroz et al. [17] (Ce-exsolution).

The benefit of the titanate phase is the relatively high electronic conductivity, compared to the CGO phase and also the higher mechanical and electrochemical stability. However, as mentioned above, titanates also show relatively low ionic conductivity (i.e., 10 times lower than CGO). Hence, the optimum composition of CGO-titanate anodes is a tradeoff that depends on the intrinsic material properties. Here we consider the option that a perovskite with higher intrinsic ionic conductivity might be available in the future as a result of the ongoing materials research (see WP 1). In this project we demonstrated with our simulations (not included in this report) that with an improved ionic conductivity of the perovskite-phase, the perovskite content for the same initial anode performance could be significantly increased. This anode composition can then potentially result in an improved stability (i.e., lower degradation rates). A perovskite with improved ionic conductivity similar to the one of CGO would enable a new anode materials design with a pure perovskite backbone impregnated with metal nano-particles (as illustrated in Fig. 6 e) or co-impregnated with CGO and metal nano-particles (illustrated in Fig. 6 f). Experimental investigations of this anode concept with perovskite-backbone and nano-particle metal impregnation [8], [18], [19], [20] or CGO metal co-impregnation [1], [7], [8], [21], [10], [9], [18] was already presented in the literature. However, the reported performances could generally not reach the same level as the state-of-the-art anodes. But this concept might get competitive as soon as a perovskite backbone with high ionic conductivity becomes available. Our simulations also show that a higher ionic conductivity in such anodes leads to an extension of the reaction zone across the anode layer, so that the effectively active surface area is also increased. Thus, achieving a higher ionic conductivity should be one of the highest priorities for the further perovskite materials development.

Another materials concept of a Ni-free anode with high performance is a pure CGO-electrode. In fact, most of the studies with a compositional variation of perovskite-CGO anodes reported the best anode performance for very high CGO-contents ([4], [3], [23] and this work). A pure CGO-anode with additional metal nano-particle impregnation is illustrated in Fig. 6 g). A low polarization resistance of such an anode was demonstrated in the present study. A further reduction of the polarization resistance is expected if a finer CGO-structure can be provided, as illustrated in Fig. 6 h). A very fine CGO-microstructure would even provide a good performance without additional impregnation of metal nano-particles, as illustrated in Fig. 6 i). In fact, Graves et al. [14] and Nenning et al. [15] reported a very low polarization resistance with pure nano-sized CGO-anodes. In the latter study, a high specific CGO-pore interface area of about 10 $\mu m^2/\mu m^3$ was achieved by a standard powder-based processing route, which resulted in a very low polarization resistance of 0.012 Ωcm^2 at T = 800 °C. For a somewhat less fine porous CGO-anode with a specific CGO-pore interface area of about 5 $\mu m^2/\mu m^3$ still a good polarization resistance of 0.17 Ωcm^2 (including the anode) at T = 800 °C was reported by Sciazko et al. [3]. However, some issues with mechanical stability and degradation behaviour were reported [3], [14] from first tests and further work is needed to study the short and long-term degradation behaviour in a systematic way. A first measure to ensure a good contact to the electrolyte was suggested by Nenning et al. [15] by PLD-deposition of a thin CGO-layer, which corresponds to the anode concept as illustrated in Fig. 6 i). Some of the problems and limitations of pure CGO-anodes can be solved by the addition of a second and more stable solid phase, which would lead back to fine porous perovskite-CGO anodes with a high CGO-content. The concept of a pure CGO-anode could be of special interest for Hexis, as it is very close to the Hexis state-of-the-art anode with CGO and a very low Ni-content. TEM-microscopy revealed that some of this

Ni is located at the CGO-surface and might contribute to electrochemical activity. A long-term test with such a CGO-Ni anode on button-cell level showed a very good degradation behaviour. Thus, an optimization of this anode especially concerning the microstructure, layer interfaces and current collection layer CCL (e.g. with a titanate-CCL) could be a valuable option.

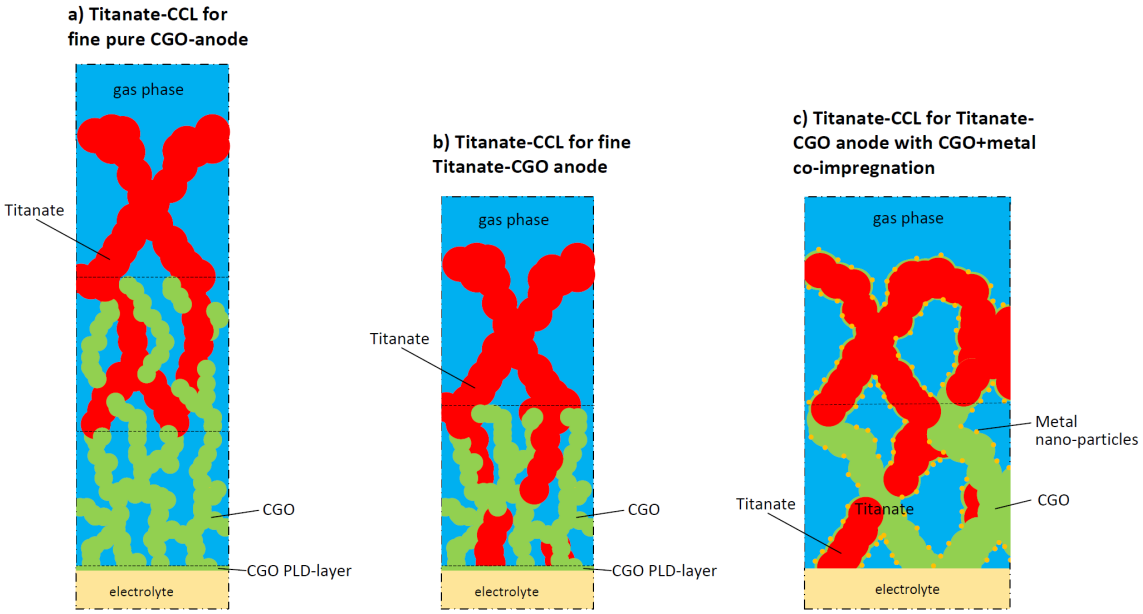

Figure 7: Graphical design guidelines for titanate current collectors layer (CCL)

Titanates can also serve as a good current collector due to their high electronic conductivity. Especially when combined with active anode layers that consist entirely of nano-sized CGO, stability problems with the current collection layer were reported if something else than a Pt current collector was used [14]. In Fig. 7 a), a ceramic material concept for the current collection layer in combination with a pure fine-porous CGO-anode functional layer is presented. In the proposed multi-layer concept, a pure CGO-layer acts as active anode. An intermediate titanate CGO adhesion layer can then ensure a stable contact to the pure titanate current collector layer on top. Note that the adhesion layer would also provide some additional electrochemical activity, which could serve as a backup for operating conditions with higher electrochemical resistance (e.g., very dry hydrogen or hydrocarbon fuels). Because of the high electronic conductivity of the titanate, the additional charge transport resistance associated with increase anode thickness caused by the adhesion layer is almost negligible. From an electrochemical point of view, the titanate phase in this adhesion layer does not need to be as fine as the CGO phase. Slightly larger pores can then be expected due to a somewhat coarser titanate phase, which is beneficial for gas transport. However, a to large difference in particle size might cause problems for the sintering, as higher sinter temperatures might be needed for the larger particles. A good composition for the adhesion layer might be around titanate:CGO = 50:50 vol.%. For the case of a fine-porous titanate-CGO functional layer as illustrated in Fig. 7 b), the titanate in the functional layer supposedly connects well with the titanate-CCL, so that no intermediate adhesion layer is required. A good composition for the functional layer is expected in the range of titanate:CGO = 40:60 vol.% (which typically corresponds to a weight ratio around titanate:CGO = 30:70 wt.%). A relatively high mechanical stability has been reported for this composition [3]. For both anode concepts that are shown in Fig. 7 a) and b) it would be favorable to use a titanate-CCL with a considerably coarser structure (compared to the anode functional layer), in order to enhance gas diffusion. However, adjacent layers with different particle sizes can be a challenge for an appropriate sintering process. From our simulations, an ideal thickness of the titanate-CCL has been estimated to be around L=20 µm when used in combination with a Ni-mesh that has a a spacing

of 170 µm. A titanate-CCL could also be beneficial in combination with a CGO-Rh co-impregnated titanate-CGO anode as illustrated in Fig. 7 c). Thereby, the current collector layer consisting of a coarse titanate backbone is also co-impregnated with CGO and metal nano-particles together with the CGO-backbone of the active anode layer. This material concept provides an additional electrochemical activity in the CCL as a backup for harsh operating conditions and/or for a WGS-reaction for hydrocarbons. The thin impregnation-coating will not affect the high effective electronic conductivity of the titanate backbone, nor does it affect the gas transport in the pores. With the CGO-Rh co-impregnation, a sufficiently high electrochemical activity can be achieved without the need of a nano-porous structure in the backbone, that can cause gas diffusion resistance associated with Knudsen diffusion in fine grained CGO anode functional layers (see e.g., 7 a and b). Hence, in the materials concept shown in Fig. 7 c), similar particle sizes in the range of 0.5 µm can be used for the CGO-AFL and for the composite-CCL, which results in a well sinterable and stable microstructure. A good composition for the backbone of the AFL is proposed in the range of titanate:CGO = 40:60 vol.% (i.e. around 30:70 wt.%). For all three suggested concepts with titanate- and composite-CCL, an appropriate contact to the Ni-mesh or interconnector must be ensured. First tests tests at Hexis indicated that this interface stability may cause some problems. A promising concept for a stable interface between current collector and Ni-mesh is based on a Ni-titanate cermet as CCL. This concept has been studied by Hexis together with the university of St. Andrews. Thus, an addition of Ni into the titanate-CCL can be a further option for the anode materials concept.

3.2.3 Conclusion and next steps

Connecting all information from experimental cell-performance characterization, literature study, microstructure analysis and modelling, design guidelines for optimized Nickel-free titanate-CGO anodes can be proposed. The design guidelines presented above represent our contribution to the final milestone M27 (deliverable D2.3) of WP2. In accordance with the working plan in Fig. 5, the remaining project-time will be used for the finalization of the PhD-thesis. The defence of the PhD-thesis is planned in spring 2023.

3.3 Current collector optimization (WP3: UMTEC, Hexis AG)

Objective

The objective of this WP is the development and application of a titanate-based material with respect to its enhanced conductivity, low chemical reactivity as well as redox stability during its application as current collector layer (CCL) at the functional anode. Especially, the microstructure stability in terms of reversibility under redox conditions (conductivity) and stability against overpotential conditions (electrolyser mode), secondary phase formation (XRD), and thermal expansion. In the final phase of the project, it is aimed the delivery of such optimised powders for industrial implementation.

3.3.1 Synthesis and evaluation of perovskite compositions: Modification of LST

On the base of our own research experiences (SFOE project SERAN, SNSF: NRP70), $La_xSr_{1-3/2x}TiO_{3-\delta}$ (LST) seems to be an ideal base composition for a material evaluation with the above-addressed performance data. Due to its perovskite phase, LST offers an exceptional structural variety for substitution with secondary elements to provide very good redox stability over a broad range of temperatures as well as oxygen partial pressure.

While the former project focussed on catalytic performance, it is now focused on a pure anode-based current collector with an appropriate, but challenging conductivity, chemical non-reactivity with common electrolyte materials, such as Cerium Gadolinium Oxide (CGO) and/or Scandium stabilized Zirconia (ScSZ), as well as redox & overpotential stability and a thermal expansion coefficient, fitting to the new HEXIS anode design. As crucial criteria, it is aimed for a 3-fold higher conductivity under equilibrium conditions (c.f. D3.2) than the substoichiometric $La_xSr_{1-3/2x}TiO_{3-\delta}$ reference.

The addressed strategy is hence to substitute an LST on the A-site (increased conductivity) and on the B-site (enhanced stability). These modifications need a reliable synthesis and processing routine since minimal deviation results in a performance lack due to secondary phase formation. Secondly, the introduction of further cations needs a highly flexible and reliable synthesis procedure for the later industrialisation step.

For clarification reasons and more details on the material strategy, we kindly ask to refer to the former report. We avoid presenting here further results on the LST presented prior to this report. However, we can confirm that the newly developed synthesis route resulted for all compositions in phase pure materials and no synthesis problems could be identified. Even more promising for WP 3.3 is the fact, that powders provided by commercial suppliers such as Praxair or PIDC – independent of the precise material composition on base of (La,Sr,Ca)(Ti,Cr)O3 – are phase pure and did not behave in any different manner, when exposed to electrolyte or anode compositions of CGO and ScSZ.

3.3.2 Evaluation of Material Properties

Material substitution-dependent conductivity data and redox stability

Pure LST is not suitable to be applied as current collector due to the loss of conductivity after redox cycling. $La_{0.2}Sr_{0.7}TiO_3$ is our reference material from prior investigations from which this LST composition showed it principal redox stability but came up with a highly insufficient material conductivity. This LST, our reference material, was improved within the project phase to an $La_{0.33}Sr_{0.50}TiO_3$ with an about 50% enhanced conductivity (c.f. annual report 2020 and interim report 2021). But even this more comprehensive LST loses about 75% of its initial conductivity with redox cycling (from 18 down to 5 S/cm).

However, this is why this project aims for A- and B-site doping to enhance material properties. From own research activities, former projects and a literature review several promising variations were identified as promising strategies to fulfil the current collector demands:

- Cr as B-site substitution (conductivity stabilisation under varying atmospheres: redox-cycling);
- Ga and Mo as B-site substitution (conductivity increase);
- Ca as an A-site substitution (conductivity increase);

The strategy is to combine stabilizing effects from Cr and enhancing conductivity effects of Ca on the A-site as well as Ga or Mo on the B-site to obtain a material with higher but redox-stable conductivity.

Activities in RESTART started towards the development of Cr-containing materials, aiming for a basic understanding of the stability effect of Cr in the LST host perovskite. The well-characterized LST perovskite with a stoichiometry of $(La_{0.3}Sr_{0.55})TiO_3$ has been chosen from that project's first phase. For the substitution of Ti by Cr, a Cr content of 5, 10, 20 50, 80 and 100 mol% was investigated. The previously described and above-mentioned new synthesis routine circumvented a critical point in the synthesis: the formation of non-conductive TiO2. But the new approach is able to produce pure titanates even at low synthesis temperatures of 650 to 900 °C, in dependency on the substitution elements.

Therefore, a series of the previously in WP3.1 mentioned A-site deficient $La_{0.33}Sr_{0.5}TiO_3$ with varying cation substitutions by Cr (LSTC) and the combinations of Cr with Mo (LSTCM), Ga (LSTCG) and Ca (CLSTC) were synthesized, analysed by XRD (phase purity), XRF (elemental compositions before and after calcination), and redox cycling in combination with conductivity measurements. Powder samples

were then processed and sintered to bars for 4-point conductivity measurement. This electronic conductivity was examined with up to 4 redox cycles and an extrapolation method was newly introduced. This method allows to estimate the equilibrium conductivity for an “infinite long” treatment time under 5% H_2 in N_2 after redox cycling, what represents the normal operation mode of a fuel cell. One should note, that the authors observed a 3 to 4 times slower reduction kinetics on dense bars than to prior samples. While titanate-based materials usually show anyhow a very slow reduction kinetic under H_2 atmospheres, the used multi-fold test setup additionally lacks of a “quick” gas exchange from redox cycling due to its large volume. Especially the revision of the test setup in 2022, that was connected to a replacement of platinum connectors and a new but significant larger tube diameter lead to even 4 times longer reduction cycles.

This means, that repetitive redox cycling (gas changes) and material screening results in very time-consuming measurements on dense bars. Here, the exponential fitting function applied – similar to the known oxygen diffusion kinetics dependency and oxygen vacancy formation – “solved” this challenge. For the later presented data, the reader should note that all conductivity values are represented by the extrapolated conductivity for an infinity time t_∞ with $t \rightarrow \infty$ and corrected bar densities (Figure 8). Moreover, a reliable bar density could be applied by a newly acquired Archimedes balance, and bar densities up to 98% could be reached, while former assumptions partly resulted in only 50% densities, making the conductivity date unreliable.

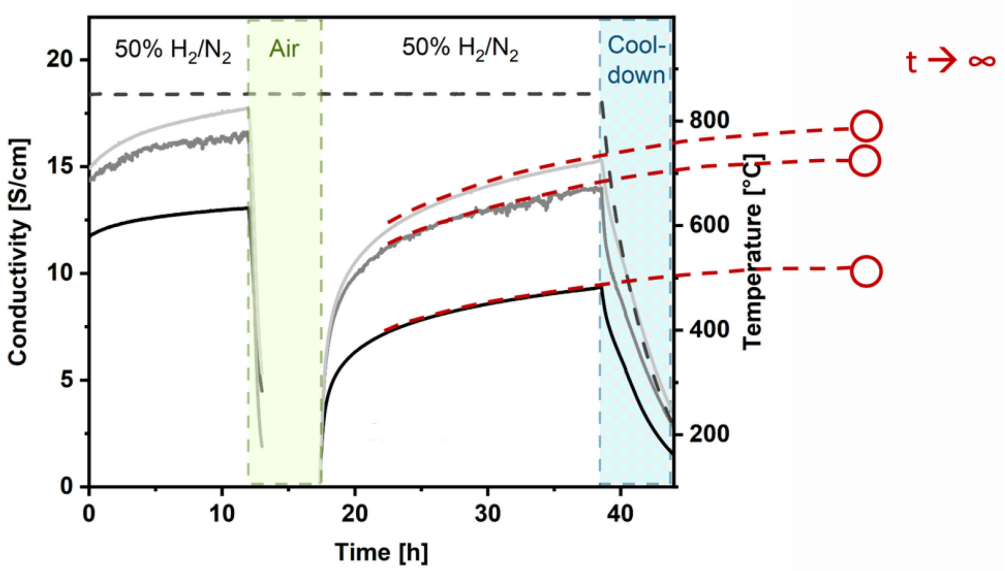

Figure 8: Temporal behaviour of conductivity under a redox cycle (black, grey and light grey curves) and the data fit with extrapolation (red).

The further aim was to enhance the performance of LST reference with Cr (LSTC) and enhance conductivity with a further substitute, i.e. Ca, Ga and Mo. A series of 4 different concentrations of the desired elements were synthesized and experimentally investigated to get a reliable impression of performance tendency. The level of substitution was carefully chosen within a reliable range, but with care not to do too much for good. The following compositions with varying substitutions were investigated:

- LST $La_xSr_{1-3/2x}TiO_{3-\delta}$ with x= 0.2, 0.3, 0.33 and 0.4
- LST**C** $La_{0.33}Sr_{0.505}Ti_{1-x}\mathbf{Cr_x}O_{3-\delta}$ with x= 0.05, 0.1, 0.2 and 0.3
- LST**CM** $La_{0.33}Sr_{0.505}Ti_{0.9-x}\mathbf{Cr_{0.1}Mo_x}O_{3-\delta}$ with x= 0.005, 0.01, 0.02 and 0.03
- LST**CG** $La_{0.33}Sr_{0.505}Ti_{0.9-x}\mathbf{Cr_{0.1}Ga_x}O_{3-\delta}$ with x= 0.01, 0.025, 0.050 and 0.075
- **C**LST**C** $\mathbf{Ca_x}La_{0.33}Sr_{0.505-x}Ti_{0.9}\mathbf{Cr}_{0.1}O_{3-\delta}$ with x= 0.1, 0.2, 0.3 and 0.4

The significant amount of conductivity data makes it necessary to report only a comprised set of material performance data. All extrapolated steady-state conductivity values are given for redox cycled materials as absolute values as observed for a maximum of 4 redox cycles. As stated prior to this report, Ga and Mo compositions did not meet expectations and were skipped.

A careful reader should note that every single data point needs up to 72 h of measurement time and more than one week of operation per sample for one redox cycle. As a conclusion, it can be stated that CLSTC (e.g. $Ca_xLa_{0.33}Sr_{0.505-x}Ti_{0.9}Cr_{0.1}O_{3-\delta}$ in blue and x = 0.1 to 0.4) performed as material with the highest conductivities but low degradation (Figure 9). Within this material composition x = 0.4 seems to be the best performing one. In contrast to that, the best Cr-free LST ($La_{0.4}Sr_{0.4}TiO_{3-\delta}$ in green) has the same or even slightly higher conductivity than CLSTC with x = 0.4, but it dramatically suffers from redox cycling. In brief, the $Ca_xLa_{0.33}Sr_{0.505-x}Ti_{0.9}Cr_{0.1}O_{3-\delta}$ with x = 0.1, 0.2, 0.3 and 0.4 (CLSTC = ~17 to 35 S/cm in blue) met the crucial conductivity criteria of a 3-fold higher conductivity than the reference LST (~5 S/cm) but present a lower conductivity drop with redox cycling. As a further outcome it was observed, that materials with a Cr content of 0.1 seem to provide a better redox stability.

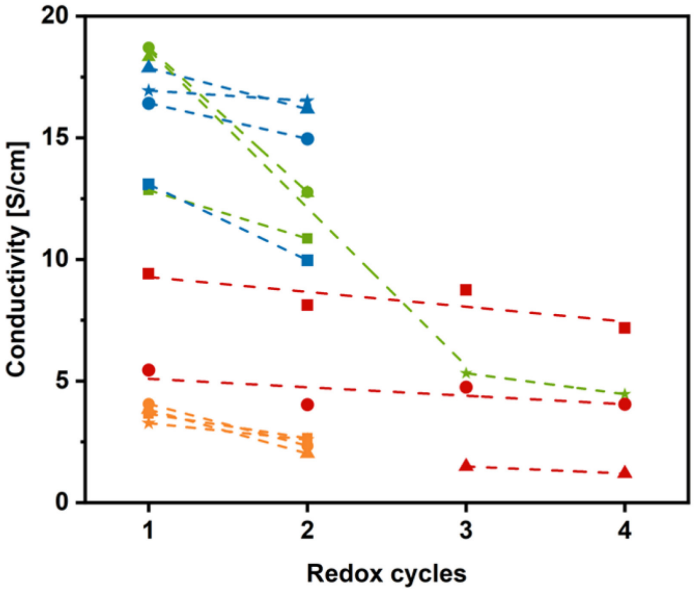

Figure 9: A comprised overview of extrapolated material conductivity of all samples prior to the setup modification as a function of redox cycles. LST: green, LSTC: red, LSTCG: orange, CLSTC: blue and sample number: ■=1, ●=2, ▲=3, ★=4 (e.g. LST ■ = LST1 with x = 0.2).

Since it was observed that a Ca content of about 0.4 seem to have the highest impact on the conductivity, and Cr = 0.1 on the redox stability (Figure 9) it was decided to further modify and vary the Cr content to scientifically explore its impact. The following materials were synthesised as further compositions to investigate variation on Ca = 0.35 – 0.68 (for conductivity) and Cr = 0.05 and 0.075 (for redox stability, Figure 10). From the sintering procedure, we can confirm that all bars do have a high density of 95% or higher of the theoretical material density, determined from XRD-based crystal data and from an archimedes principle based balance.

- $Ca_{0.4}La_{0.2}Sr_{0.3}Ti_{0.9}Cr_{0.1}O_3$
- $Ca_{0.4}La_{0.25}Sr_{0.275}Ti_{0.9}Cr_{0.1}O_3$
- $Ca_{0.35}La_{0.33}Sr_{0.15}Ti_{0.9}Cr_{0.1}O_3$

- $Ca_{0.45}La_{0.33}Sr_{0.05}Ti_{0.9}Cr_{0.1}O_3$
- $Ca_{0.4}La_{0.33}Sr_{0.1}Ti_{0.925}Cr_{0.075}O_3$
- $Ca_{0.4}La_{0.33}Sr_{0.1}Ti_{0.95}Cr_{0.05}O_3$
- $Ca_{0.4}La_{0.33}Sr_{0.1}Ti_{0.9}Cr_{0.1}O_3$
- $Ca_{0.56}La_{0.2}Sr_{0.14}Ti_{0.9}Cr_{0.1}O_3$
- $Ca_{0.68}La_{0.1}Sr_{0.17}Ti_{0.9}Cr_{0.1}O_3$
- $Ca_{0.5}La_{0.33}Sr_{0.00}Ti_{0.9}Cr_{0.1}O_3$
- $Ca_{0.5}La_{0.28}Sr_{0.08}Ti_{0.9}Cr_{0.1}O_.$

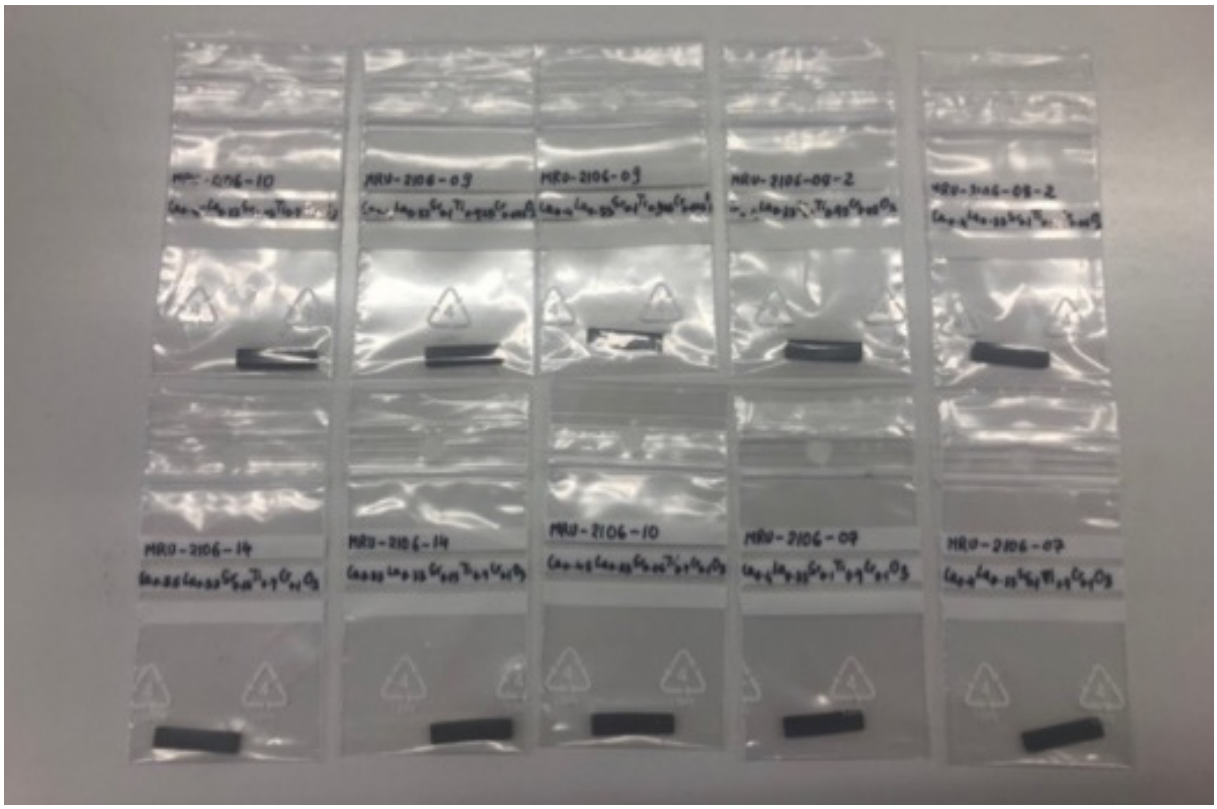

Figure 10: Pressed, sintered, and pre-reduced bars of new Ca compositions ready for conductivity measurements.

REMARK: At this point it has to be commented that a setup modification was necessary and executed at Hexis in spring 2022, improving the measurement quality and thus generating higher quality data when compared with the old setup. The refurbishment resulted in a new setup with longer equilibrium times for a gas exchange and to reach steady state conditions. However, reliable conductivity measurements are more crucial since it is the main property to be affected by the composition variations. However, several measurements could be carried out, but also several compositions remain unmeasured because from July 2022 on, the setup could not be used anymore from the well-known reasons.

Figure 11 (left) shows all measurements carried out with the new setup. The conclusion which can be made is, that changing the B-site Cr from x = 0.1 to 0.075 or even 0.05 lead to a significant conductivity

drop, e.g. for $Ca_{0.4}La_{0.33}Sr_{0.1}Ti_{0.95}Cr_{0.05}O_3$ (black) from 13 S/m down to 5 S/m. On the other hand, a Cr content of x = 0.1 stabilizes the conductivity under redox cycling, even for low performing materials such as $Ca_{0.68}La_{0.1}Sr_{0.17}Ti_{0.9}Cr_{0.1}O_3$ (light green). This proofs our recently stated assumption that a CLSTC material composition need a minimal Cr content of 0.1 on the B-site to achieve redox stability throughout redox cycling.

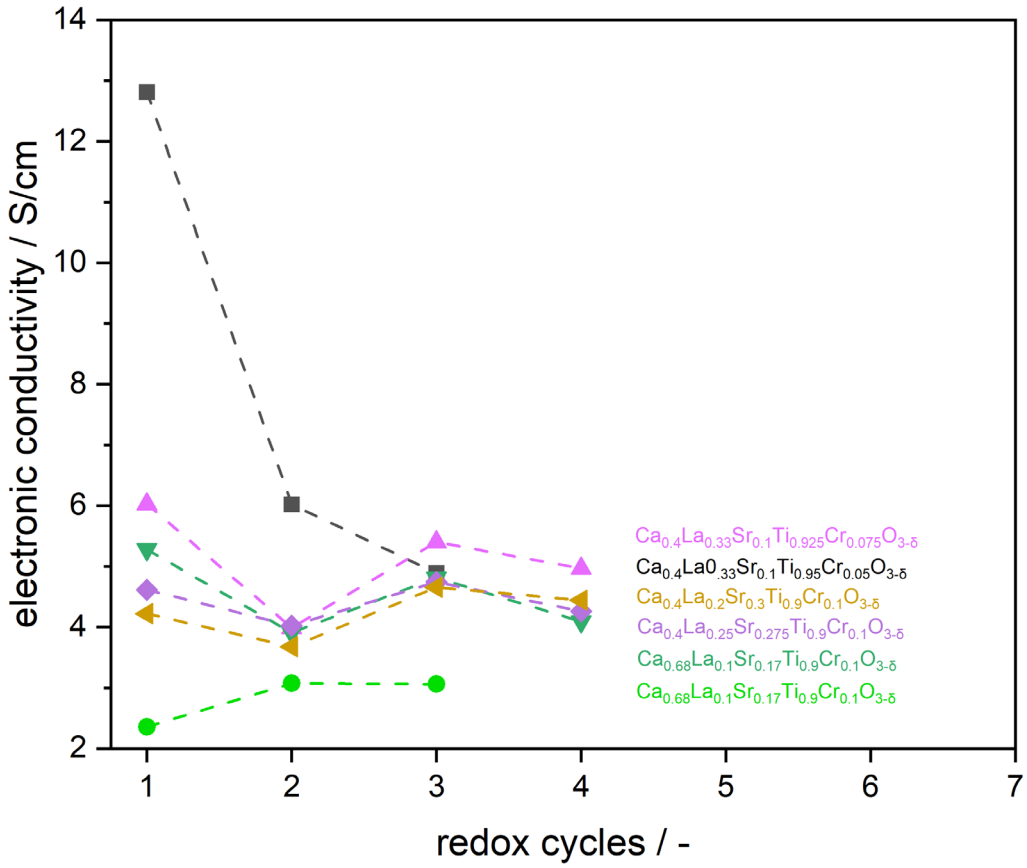

Figure 11: Extrapolated material conductivity of CLSTC samples as a function of redox cycles.

Finally, it was possible to re-evaluate formerly measured and well performing samples in the new setup. Also, a more reliable density acquisition turned out, that especially the $Ca_xLa_{0.33}Sr_{0.505-x}Ti_{0.95}Cr_{0.1}O_3$ seem to perform better than formerly calculated (Figure 9). So far, we can correct CLSTC to the values, as shown in Figure 12. The only uncertainty is connected to CLSTC with x = 0.4 for which a further exploration of performance data is needed. This will be finished until the final report and redox cycling of these samples will be finished as soon as the setup is accessible. Currently, conductivity measurements for all CLSTC compositions and a Sr-free sample (CLTC) are in the improved setup and waiting for the measurement.

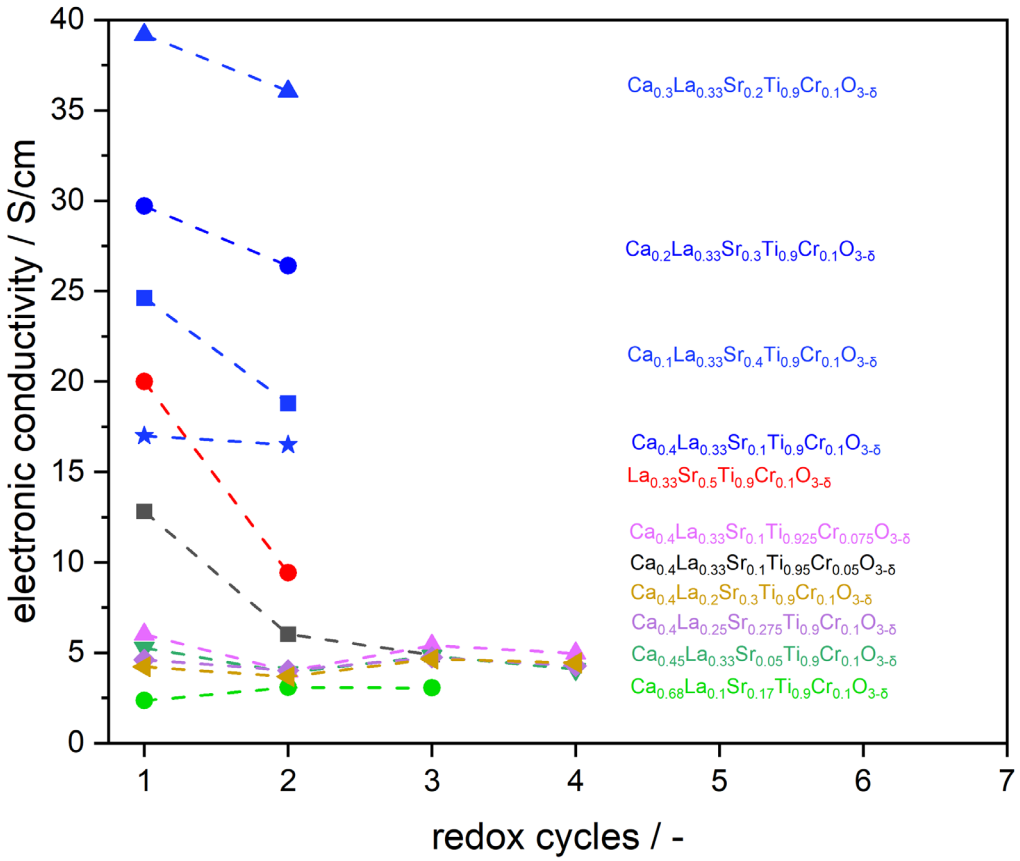

Figure 12: Conductivity values from the new setup and re-evaluated CLSTC (0.1, 0.2 and 0.3) for maximum 4 the redox cycles. Remark: CLSTC for Ca = 0.4 is still “uncorrected”.

Chemical compatibility with anode (CGO) and electrolyte (ScSZ) materials

Since the current collector gets in intimate contact with the anode (CGO) and electrolyte materials (ScSZ), phase stability and low chemical reactivity are crucial. Therefore, all promising current collector compositions were subjected to a so-called chemical “rapid screening” procedure with typically applied CGO and ScSZ powders from Hexis’ material provider. Our phase pure current collector nanopowders with a high specific surface area were mixed with CGO and ScSZ powders and undergo a temperature procedure at which secondary phases potentially can be formed. The high surface area leads to a large number or contact points, and reaction zones between the particles. Secondly, small nanoparticles typically have defects on the surface from the strong curvature. These defects are primary zones for unwanted reaction products.

Initial LST samples were therefore analysed by XRD after a temperature treatment: Powders were mixed, mortared and pressed to pellets for an intimate contact before sintered for 12 h at 1300°C in air (high temperature at high p_{O2}). XRD phase analysis will then indicate any phase changes from chemical reactions. Figure 12 shows the XRD pattern of mixed specimen powder composites from the reference LST and CGO as well as ScSZ.

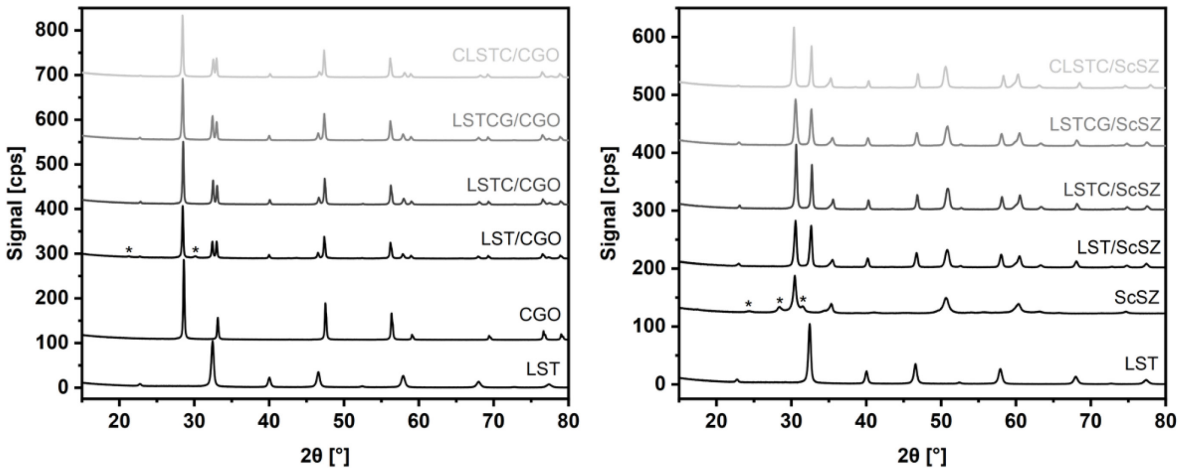

Figure 13: XRD pattern of all co-substituted LST/CGO composites (weight ratio 1:2) after sintering (left). XRD pattern of all LST/SCSZ composites (weight ratio 1:2) after heat treatment. Pure LST1, CGO and ScSZ are given as references on the bottom (left and right). * indicated phase impurities in LST (left) or in the commercial ScSZ material (right).

The LST reference is very stable under the investigated conditions and neither newly formed reaction products nor secondary phases are observed. It has to be noted, that there is only one exception from the LST composition calcined at 750°C. This LST powder has some higher amorphous content, leading to reflections at 2Θ = 21.33°, 30.12°, 43.64° and 65.61° assigned to $LaTiO_7$. But $LaTiO_7$ does not contain any Ce or Gd, hence this phase is not formed from the contact with CGO. In contrast to this, some secondary ZrO_2 reflections were observed for the commercial ScSz in the as-provided condition. This secondary phase can be attributed to monoclinic segregated ZrO_2 that is thermodynamically stable at temperatures up to 1170°C, however, at the conditions applied in these initial experiments (1300°C) a transition to a tetragonal phase is observed with the vanishing of all the additional reflections, even if in close contact with LST.

As for the new CLST compositions, the chemical compatibility with the anode and electrolyte were also investigated but at 1200°C and for 4 h of reactivity time, to be closer on the real application conditions for the cell production. The results are shown in Figure 13 and Figure 14, respectively.

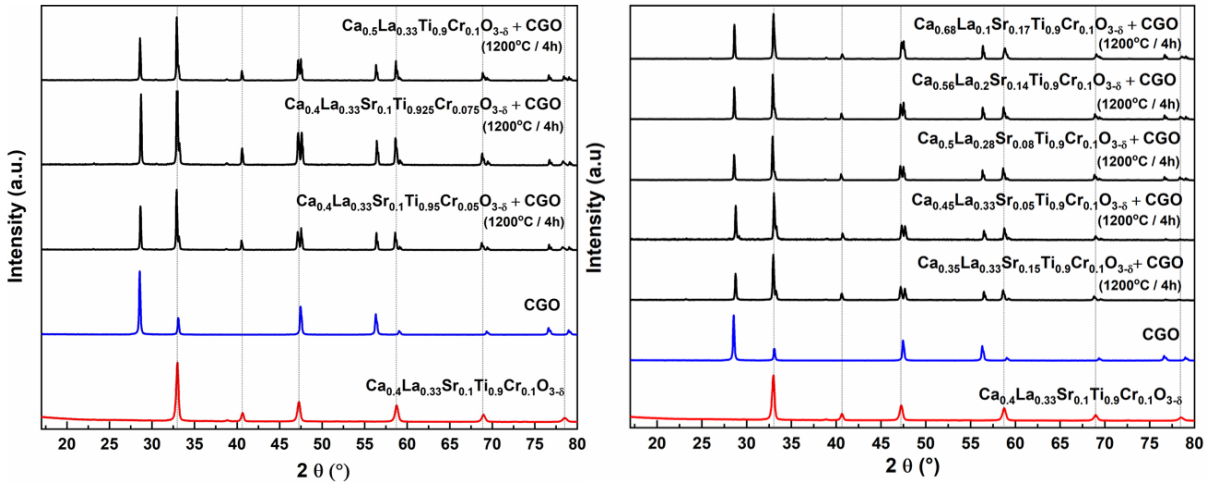

Figure 14: XRD patterns for the prepared CLSTC and CLTC (Sr-free) samples after "rapid screening" experiment with CGO. $Ca_{0.4}La_{0.33}Sr_{0.1}Ti_{0.9}Cr_{0.1}O_3$ composition used as reference material.

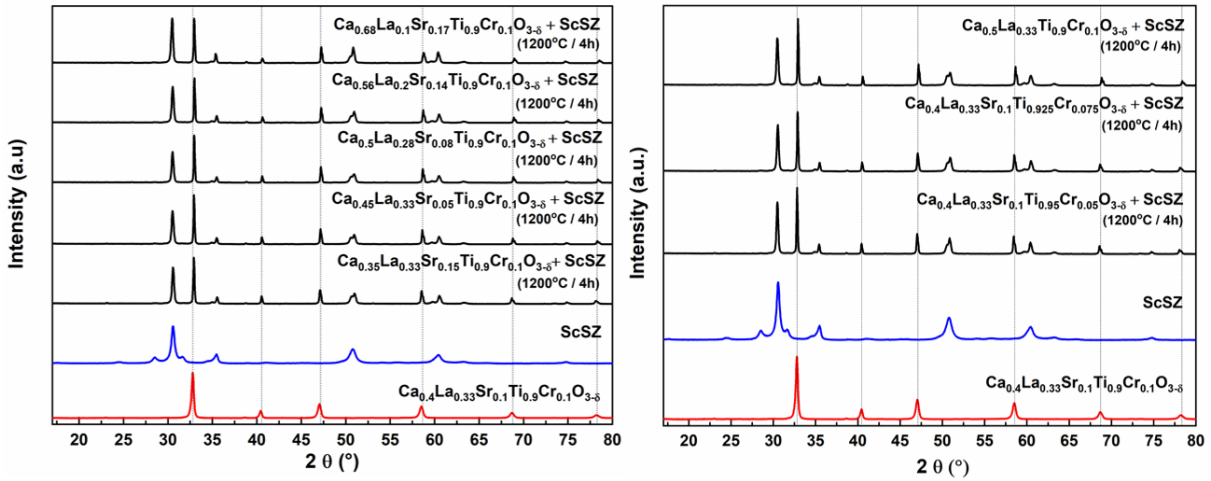

Figure 15: XRD patterns for the prepared CLSTC and CLTC (Sr-free) samples after "rapid screening" experiment with ScSZ. $Ca_{0.4}La_{0.33}Sr_{0.1}Ti_{0.9}Cr_{0.1}O_{3-\delta}$ composition used as reference material.

The encouraging XRD-based phase analysis shows that all compositions do not react with CGO and ScSZ under industrial manufacturing conditions. Only reflections associated with the CLSTC reference compositions as well as CGO or ScSZ were observed. The purely ZrO_2-related impurities disappeared again after temperature treatment (Figure 14) similar to the cell fabrication conditions which are more severe than operation.

3.3.3 Powder supply to the industry partner

It was determined in the RESTART project meeting at 22.06.2022, that a first batch of about 20 - 30 g of the best performing CLSTC is provided to Hexis for a button cell or short stack production. The results of the next batch of samples measured according to its conductivity should have been used to decide about the final upscaled CLSTC powder production. Since the upscaled powder samples – according to the current state of knowledge – cannot not be used for production of button cells and measured at the industry site, it was not decided on the final composition and upscaled.

3.4 Scalability of Cell manufacture (WP4: Hexis)

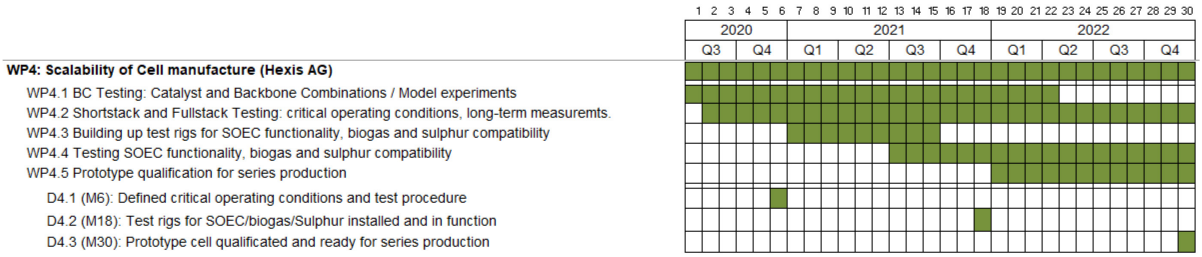

Figure 16: Gantt-chart and deliverables for work package 3 (scalability of cell manufacture)

3.4.1 BC Testing: Catalyst and Backbone Combinations / Model experiments

To investigate several different samples in this RESTART project with variations in catalyst and backbone combinations, as well as current collector layers, one basic work is to have one or two long-term reference measurements. With them we are able to evaluate performance and especially the degradation behaviour of samples, compared to Hexis' standard cells.

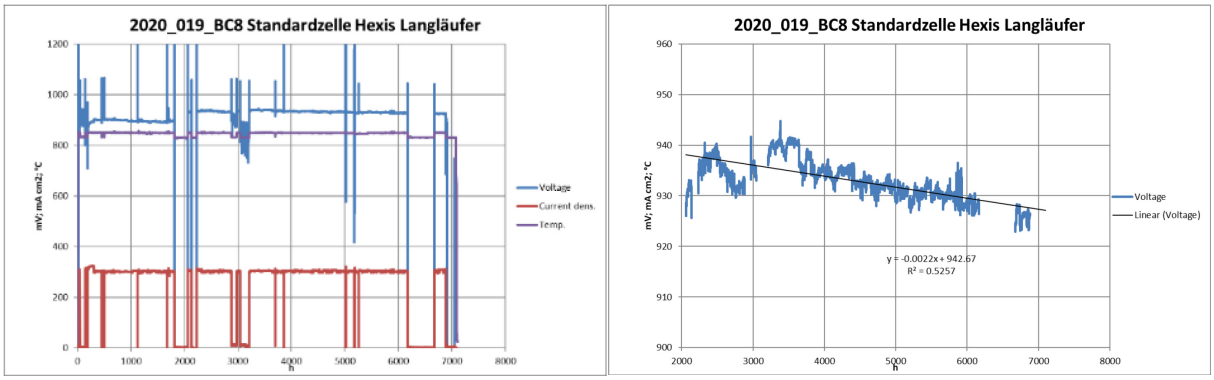

Figure 17: a) Long-term performance and b) zoomed degradation behaviour of a Hexis standard button cell. With almost 7.000 hours, the degradation rate is about 0.2%/kh.

A comparison between the Figures 17 and 18 shows that a multilayered Rh titanate anode (1st layer: pure CGO, 2nd layer: LSCT 40%: CGO 60%, 3rd layer: pure LSCT) cell has a tendency to higher degradation rates, and additional button cell runs have to be performed to confirm this tendency.

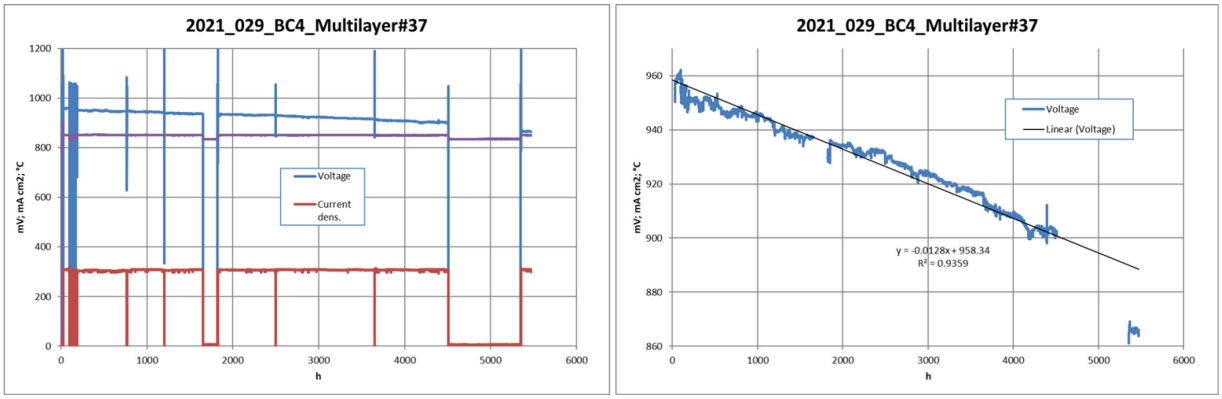

Figure 18: a) Long-term performance and b) zoomed degradation behaviour of a multilayered LSCT/CGO button cell. Until almost 5.500 hours, the degradation rate is about 1.4%/kh.

3.4.2 Shortstack and Fullstack Testing: critical operating conditions, long-term measurements

Some results from Shortstack testing are already shown in WP1.1 (chapter 3.1.2). A fullstack with the Rh inkjet impregnated titanate cells from iPrint was started in May 2022 but had to shut down after almost two weeks of operation because of one cell with poor performance (Figure 19). There was no clear indication on the failure cause, but it seemed to be a gas depletion in the first cell at the bottom of the stack which is not related to the cell itself, but possibly to the test conditions.

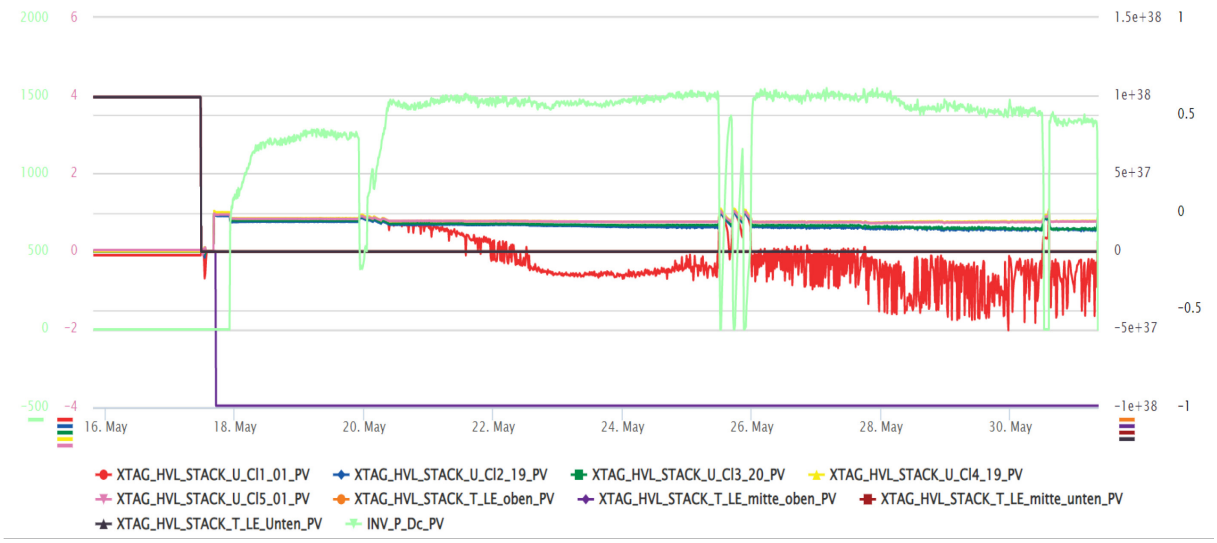

Figure 19: Fullstack system test with 60 Rh inkjet impregnated titanate cells. The overall stack performance is satisfying, but cell 1 shows significant failure signals.

The one “bad” cell has to be replaced and the stack was restarted by the end of June 2022. Since all test benches were stopped in early August 2022, there is no valuable data to show here.

3.4.3 Building up test rigs for SOEC functionality, biogas and sulphur compatibility

A button cell test rig has been modified to test cells for SOEC functionality (Figure 20). On the anode side of SOF cells, which is the cathode side for SOE cells (when I report about SOEC results, I will call this side the “fuel electrode”, and the other the “air electrode”), a source of water steam has to be implemented. This was done by providing a hydrogen gas pipe and an air gas pipe. Both gases can be mixed through a t-piece, 20 cm before the mixture is introduced into the hot furnace. To promote the oxyhydrogen reaction, a platinum wire was placed inside the ceramic inlet pipe.

Figure 20: Modified button cell test rig for SOEC measurements

The biogas and sulphur compatibility are planned to be tested later this year on the shortstack scale.

3.4.4 Testing SOEC functionality, biogas and sulphur compatibility

Button cells with different compositions were tested and voltage-current-measurements were performed (Figure 21).

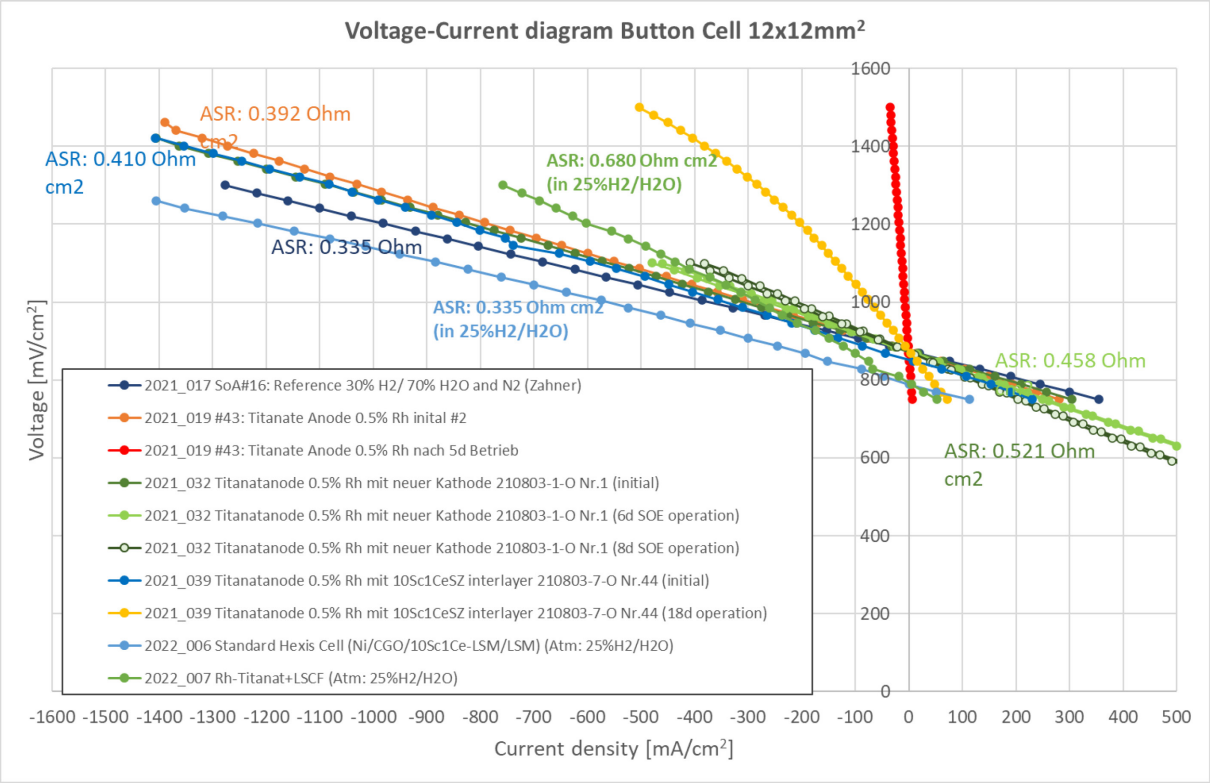

Figure 21: Voltage-Current diagram of selected button cell samples, showing the cell performance in SOEC and SOFC mode. Fast degradation phenomenon is observed after few hours of operation.

As previewed in the last interim report, potentiostatic SOE measurements are performed (Figure 22). The most cells showed severe degradation despite different fuel electrodes, air electrodes, gas atmospheres, and voltage conditions (closer or further away from the thermoneutral voltage of 1.28V). First postmortem analyses showed no clear indications for the degradation mechanisms.

The latest measurements employed an air electrode containing of a CGO layer on the electrolyte and a LSCF layer (a La-Sr-Co-Fe perovskite) on top of it. This sample started with higher ohmic resistance (lower current density at a given voltage) than the previous tested air electrodes. But amazingly, the degradation stability is much higher than the others.

As the optimization of the air electrode is not in the focus of this project, some of the next samples are planned to keep the CGO/LSCF air electrode constant and test different fuel electrodes (e.g., Rh titanate vs. standard CGO electrodes) on the SOE button cell rig.

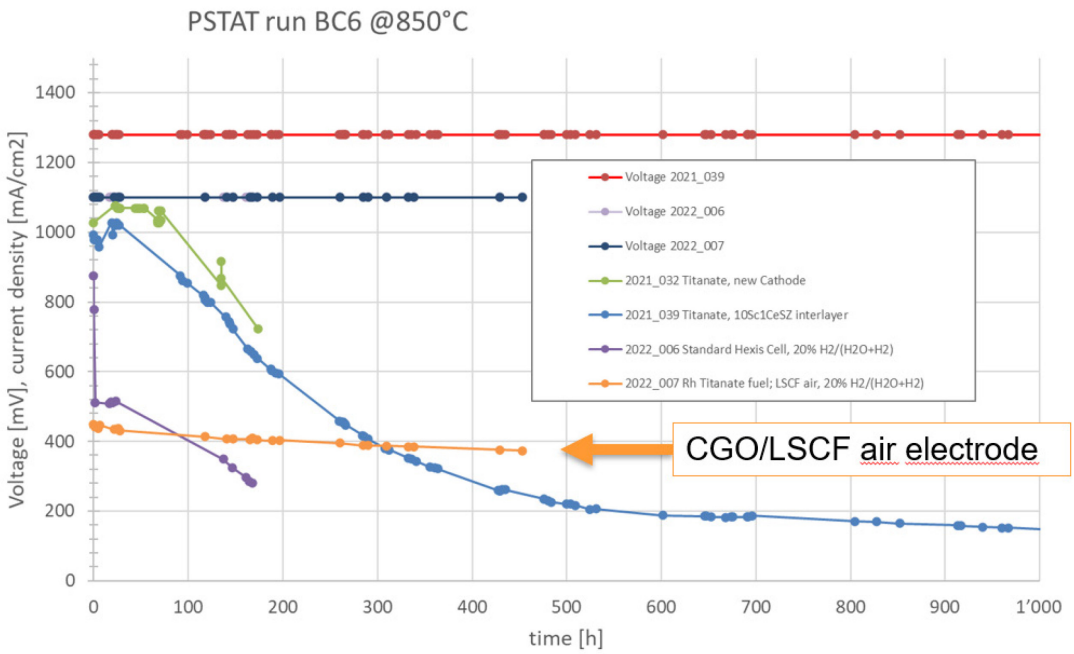

Figure 22: Potentiostatic voltage-current diagram showing degradation behaviour for different button cells under SOE conditions.

3.4.5 Prototype qualification for series production

A series production of catalyst impregnated titanate cells will not be realized in this project. Instead, a series of cells from the feasibility study with iPrint, is being tested on the system scale. It is planned to run a pure titanate anode cells full stack (as already described in chapter 3.4.2) as a long-term (degradation) measurement. Another full stack with mixed cells (Standard Hexis anode / Rh titanate anode) is planned for a system run with a combination of thermoredox cycling, overload conditions, and other simulated incidents to examine the robustness of the new cells compared to the standard cells.

3.5 Microstructural investigation (WP5: ICP ZHAW)

3.5.1 Overview of workplan and deliverables

The main task of WP5 is to to characterize anode microstructures at different length scales (WP5.1: layer scale, WP 5.2: pore scale and 5.3: nano-scale) by means of electron microscopy, tomography and image processing/image modelling. The information gained with microscopy represents the basis for knowledge-based microstructure optimization by means of digital materials design (WP 5.4: DMD). The thus determined effective properties for different microstructures are used as input for the multi-physics electrode model in WP2, which provides a prediction of the corresponding anode performances (ASR). In this way, DMD is capable to provide design guidelines for improved anode microstructures (pore scale), for improved anode architectures (layer scale) and for optimized catalyst impregnation (nanoscale). This also leads to the formulation of design guidelines for anodes with higher initial performance and improved long term stability, as discussed in this report in WP2.

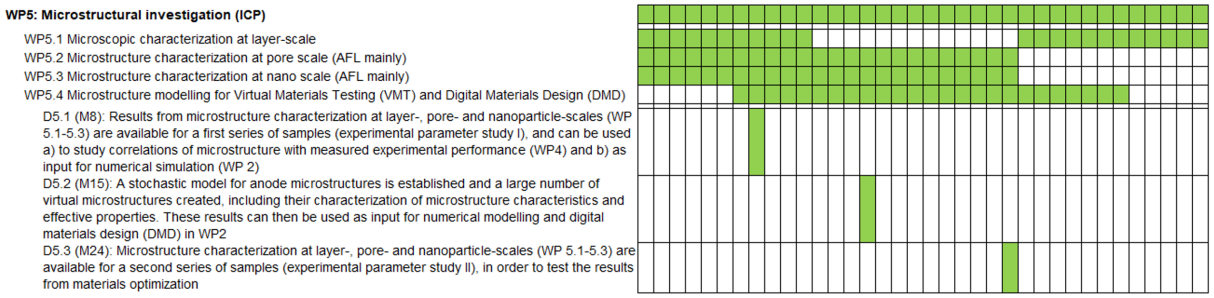

Figure 23: Gantt-chart and deliverables for work package 5 (microstructure investigations)

3.5.2 Virtual Materials Testing and Digital Materials Design

A fundamental aim of this project is to establish a methodological platform for systematic microstructure optimization based on the integration of various modelling tools. This modelling platform is called digital materials design (DMD). The workflow linking these different modelling tools is illustrated in Fig. 24.

The DMD platform is now fully established and is used for the elaboration of design guidelines for optimized anode microstructures. Thereby some of the modelling tools were established in WP2 and some in WP5. The descriptions of the various tools contributing to the DMD platform are currently in preparation for dedicated publications (will also appear as chapters in the PhD thesis of Philip Marmet). The following publications (with working titles) are currently in preparation:

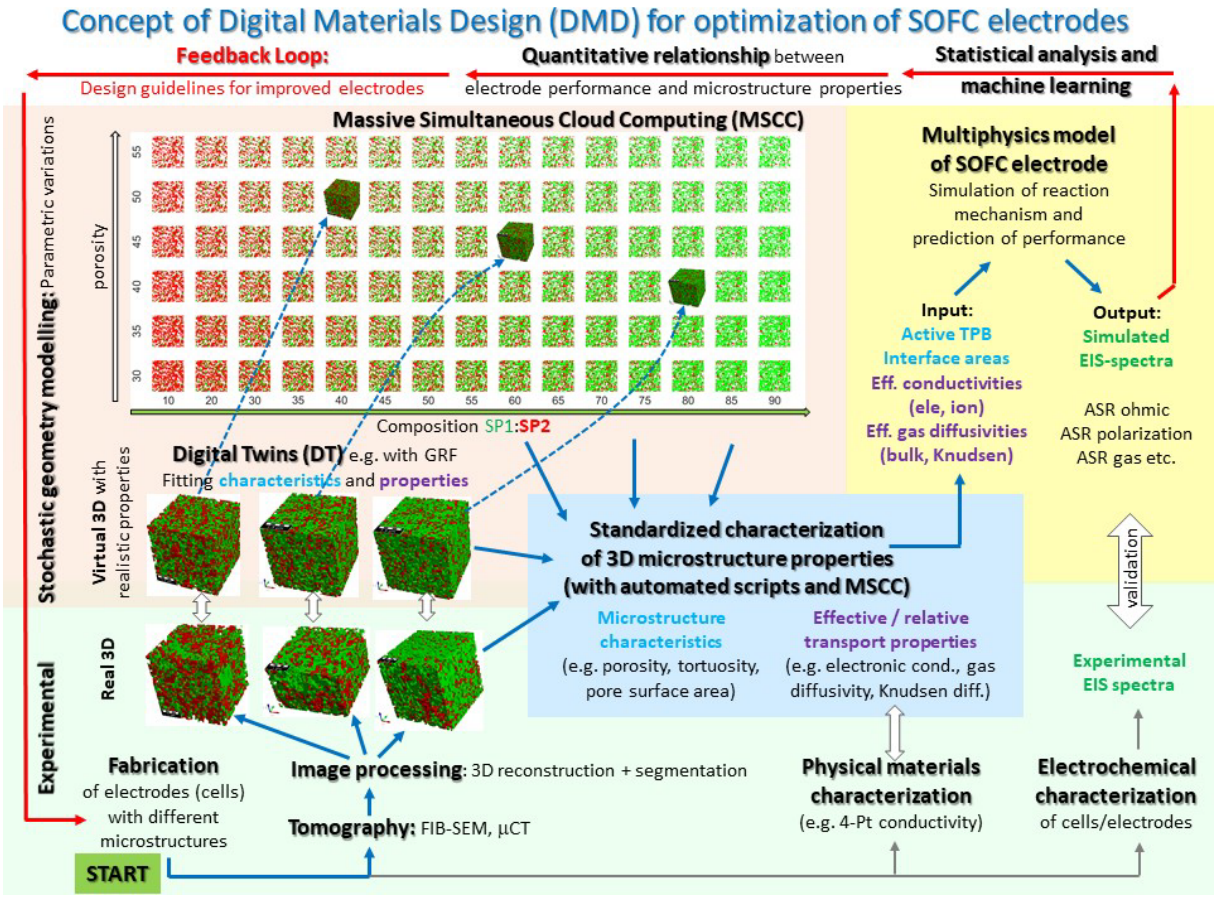

Figure 24: Overview of methodologies for Digital Microstructure Design (DMD).

Standardized microstructure characterization of SOFC electrodes as a key element for Digital Microstructure Design (See blue domain in fig. 24)

This tool provides a thorough characterization of all relevant microstructure characteristics such as tortuosity, constrictivity, size distributions, volume fractions, surface and interface areas, TPBs, hydraulic radii of the different phases (CGO, titanate, pores) and all relevant effective/relative properties such as electronic and ionic conductivities, gas diffusivity and permeability for composite SOFC electrodes. The underlying script consists of numerous image analysis procedures and numerical transport models, which are running fully automatically, - either for single 3D images on a local server or for jobs with a large number of 3D images in the cloud. The time to characterize thousands of different 3D structures by massive simultaneous cloud computing (MSCC) is now almost the same as the time for characterization of a single 3D structure on a local server. This time reduction is a basic precondition for and, hence, a major step towards data-driven materials optimization with DMD.

Stochastic microstructure modeling of SOFC electrodes based on a pluri-Gaussian approach

(See red domain in fig. 24) Stochastic geometry modelling needs to be fitted to real microstructure data from tomography in order to create virtual microstructures with realistic properties. This fitting is done for a relatively small number of tomography data, since experiment-based tomography is time consuming and expensive. The resulting digital twins are virtual microstructures, which reveal the same properties as the real ones from experiment, but which are created based on a set of stochastic parameters. In this way a stochastic model is fitted to reality. A large number of virtual microstructures with realistic properties can then be created by variation of stochastic parameters (i.e., interpolation between and extrapolation beyond the composition of the fitted digital twins). An example was shown in the previous report (WP2), whereby composition and porosity are varied systematically. Further parametric variations that are currently investigated by means of stochastic modelling and DMD are particle size of titanate, infiltration of CGO and anode thickness (see also presentation and discussion in PhD Philip Marmet). The methodologic approach is based on pluri-gaussian random fields. An important advantage of this approach consists in the capability to create a large number of virtual but realistic microstructure in much shorter time than e.g., with conventional particle packing approaches. The fast realization of a large number of 3D structures is again a basic precondition for and, hence, a major step towards, data-driven materials optimization with DMD.

Ionic and electronic composite conductivity of MIEC-based SOFC electrodes: Implications for microstructure optimization

In composite MIEC anodes (such as CGO-titanate) the specific charges (i.e., either electrons or ions) are transported in both solid phases, although their transport preferentially takes place in the phase with higher intrinsic conductivity (i.e., titanate has higher intrinsic conductivity for electrons, CGO for ions). This leads to special microstructure effects, which cannot be observed in composite electrodes with single phase conductors (e.g. Ni-YSZ). Such special effects are the bridging of disconnected islands, dead ends and bottlenecks by the complementary phase. These characteristic properties of MIEC electrodes are described as ‘composite conductivity’. The combined effects from MIEC microstructures and intrinsic properties on composite conductivity are discussed in a dedicated paper (also available as a chapter in the PhD). It includes a discussion of the influence of composite conductivity on the corresponding design space in composite MIEC electrodes.

Multiphysics model of MIEC based anodes (See yellow domain in fig. 24)

A model for CGO anodes has already been published (see Marmet et al. 2020, PhysChemChemPhys [1]). This model was extended for CGO-titanate composites and validated with experimental data. Based on the input from standardized characterization and stochastic modelling, the performance of anodes

with varying microstructures can be predicted reliably, including a simulated impedance spectra and various ASR components (polarization components at different frequency ranges).

Concluding paper on titanate-CGO anode optimization by digital materials design (DMD)

As a final chapter and concluding paper, a summary of the project outcome is currently in progress. Thereby, it is demonstrated how the powerful capabilities of the DMD platform can used for optimization of CGO-titanate anodes. Digital twins were fitted to FIB-SEM data. A large number of realistic microstructures were created with the fitted stochastic model, and their properties and performances were predicted with the established tools for characterization and electrode modelling. The effect of tuning different microstructure features was virtually tested and corresponding possibilities for improvement were identified. Design guidelines for optimized titanate-CGO electrodes were presented in WP2 in this report as an outcome of the DMD-process and from literature work. Even though not all the planned experiments for the verification of these design guidelines could be realized, they can guide the activities of Hexis towards further improvements of the composite MIEC anodes for higher performance and also for higher robustness. For future developments, the DMD platform offers unique capabilities also for the optimization of other types of electrodes (e.g., cathodes) and for other applications (e.g., SOEC, reversible SOC, battery electrodes etc.).

3.5.3 Conclusion and next steps

All the milestones of WP 5 (M8, M15, M24) have been successfully accomplished. As reported in previous reporting periods, microstructure properties have been studied on layer scale, pore scale and nano scale for an initial series of samples (M8) and for a second experimental study with systematic variations of the microstructures (M24). Stochastic models for a virtual but realistic microstructure variation have been developed and applied for the optimization of the LSCT-CGO anodes (M15). The remaining time of the project will be used for the publishing of the research results in peer-reviewed journals and for the finalization of the PhD-thesis of Philip Marmet.

3.6 Catalyst optimization (WP6: Hexis)

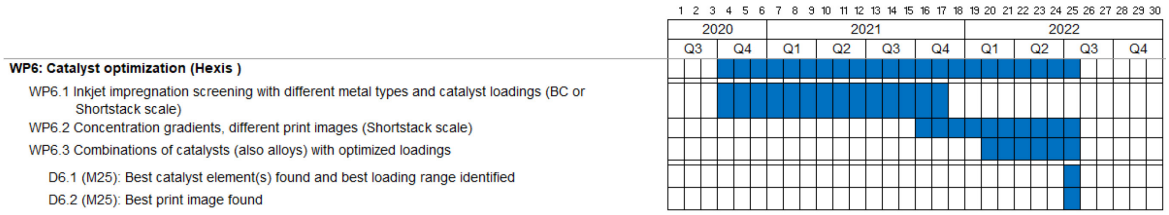

Figure 25: Gantt-chart and deliverables for work package 6 (Catalyst optimization)

The activities in WP6 were mainly carried out in collaboration with Hexis' cooperation partner USTAN (University of St. Andrews, Scotland).

In WP6.1, investigations were initial started on a button cell level with Pd and Ru as catalysts, but we decided to proceed directly with the full cells on the Shortstack scale, where we screened the following catalyst elements: Pt, Pd, Ru, Fe, Mn, Ni.

For WP6.2, the production of full-cell samples by USTAN was planned, but was postponed in favour of the full cells of WP6.1. Colour gradients and print image investigations will be realised in the upcoming Innosuisse project, where industrial inkjet printheads can serve this purpose much better.

WP6.3 Catalyst combinations and optimised catalyst loading tests will be realised in the upcoming Innosuisse project, where industrial inkjet printheads can more conveniently fulfil this purpose.

3.6.1 Screening of catalyst elements

Three shortstack measurements are performed with following cells:

Figure 26: cells 1+4: 0.2% **Fe** impregnation on double layer LSCT 40% / CGO 60% backbone
cells 2+5: 0.2% **Pd** impregnation on double layer LSCT 40% / CGO 60% backbone
cell 3 (Ref): 0.2% **Rh** impregnation on double layer LSCT 40% / CGO 60% backbone

Figure 27: cells 1+4: 0.2% **Ru** impregnation on double layer LSCT 40% / CGO 60% backbone
cells 2+5: 0.2% **Pt** impregnation on double layer LSCT 40% / CGO 60% backbone
cell 3 (Ref): 0.2% **Rh** impregnation on double layer LSCT 40% / CGO 60% backbone

Figure 28: cells 1+4: 0.2% **Mn** impregnation on double layer LSCT 40% / CGO 60% backbone
cells 2+5: 0.2% **Ni** impregnation on double layer LSCT 40% / CGO 60% backbone
cell 3 (Ref): 0.2% **Rh** impregnation on double layer LSCT 40% / CGO 60% backbone

Short summary of the results:

All three measurements show that there is no competing catalyst element for Rh. In all three runs, an Rh impregnated anode still has the best and most robust performance.

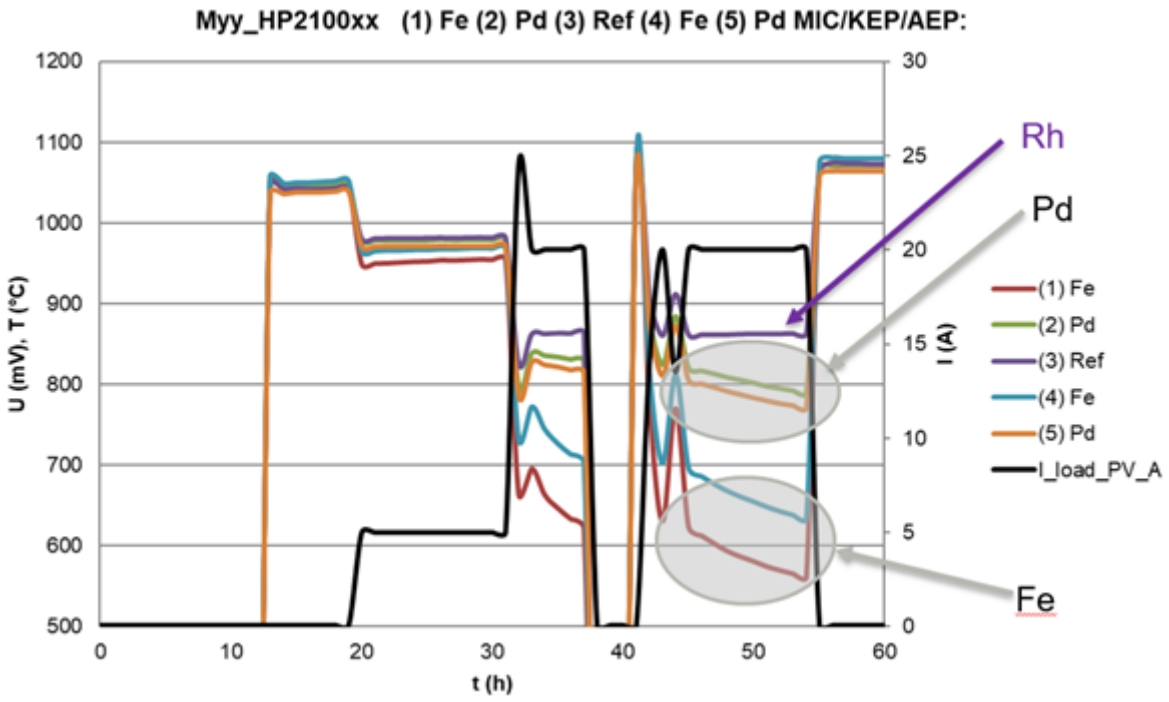

Figure 26: Shortstack run comparing Fe, Pd, and Rh impregnated titanate backbones

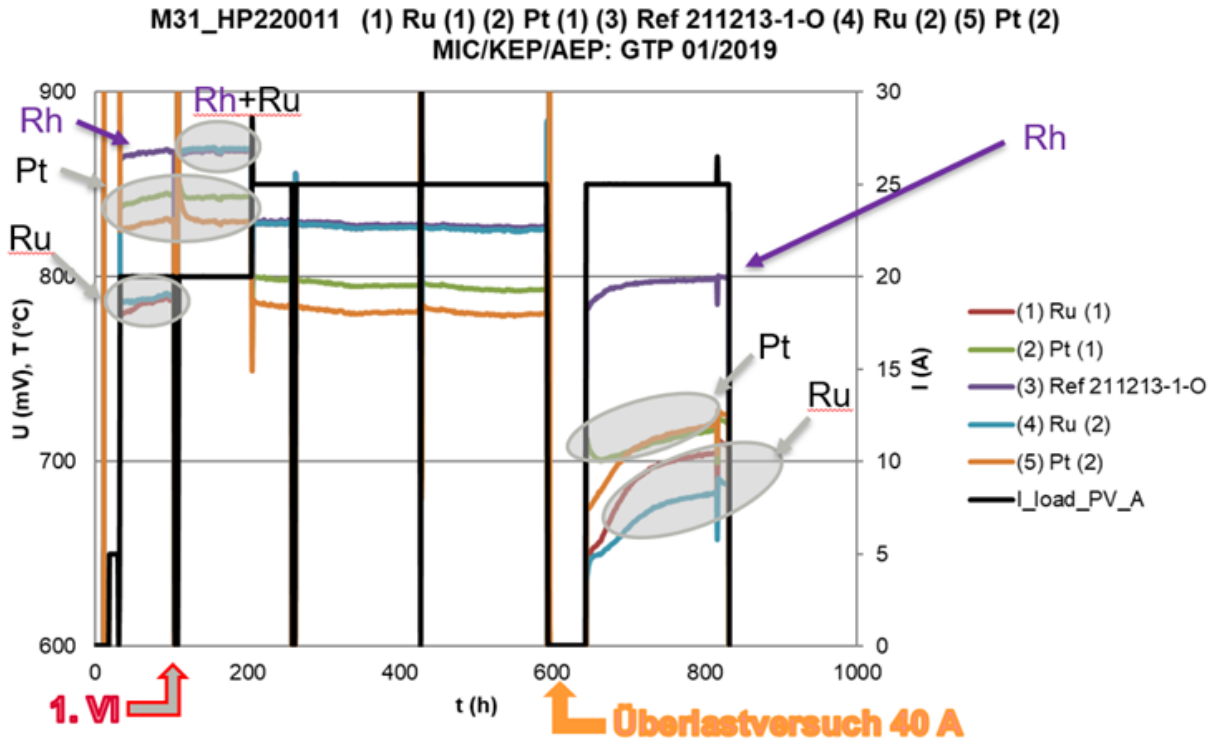

Figure 27: Shortstack run comparing Ru, Pt, and Rh impregnated titanate backbones

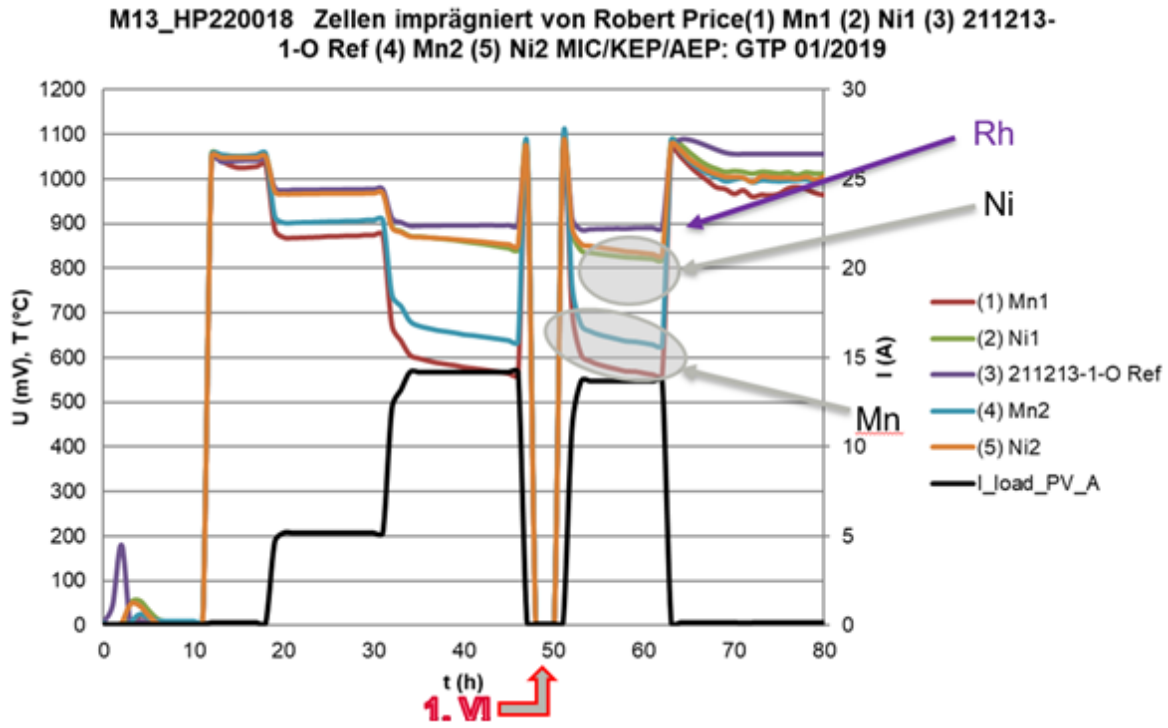

Figure 28: Shortstack run comparing Mn, Ni, and Rh impregnated titanate backbones

4 Evaluation of results to date

Overall, the project is progressing towards the set goals.

Shortstack measurements showed that there is potential for improvement when impregnating Rh catalyst on anode backbones on a laboratory level. The impregnation depth is a major parameter in the preparation of full cells. This insight has been incorporated into the feasibility study on inkjet impregnation (with iPrint). The catalyst solution could be applied in one pass and with the right amount and composition of solutions used. The such produced cells were then verified by Shortstack tests to show sufficient electrochemical performance. The start of development of a prototype production equipment is planned for summer 2022 in the framework of an Innosuisse project.

The evaluation of EIS data from various button cell measurements, microstructure analysis and advanced modelling already successfully led to suggestions for optimized anode designs (e.g., multilayer cells), which will be further verified by button cell and shortstack measurements.

To find the best suitable perovskite titanate material, a screening process was initiated, where a series of different material compositions could be synthesized. The results from bulk electrical conductivity measurements showed promising candidates for further verification also of nearby compositions. The electrical conductivity of thin anode layers is planned to be measured on such compositions and compared to those of LSCT.

Button cell measurements of Hexis standard cell materials have set the bar for further investigations on Rh titanate anode materials in terms of initial performance, degradation, and stress test behaviour. A series of button cell samples with variations of the anode backbone was prepared and measured. The resulting data feed the modelling works in WP2, leading to a more fundamental understanding of the function of the novel anodes.

A SOEC test rig was built up and some promising results are shown. The steam which is needed for electrolysis conditions is generated by a mixture of hydrogen and air that is guided through the hot zone in the furnace. The setup is working in a satisfactory manner.

Microstructure analysis on the nano scale and pore scale showed interesting findings for catalyst distribution, backbone composition and its microstructure. Data also flowed into WP2 and give incentives for further anode design.

In WP6, a screening of different catalyst element impregnations showed that Rh is still the most promising candidate in terms of performance and robustness.

5 Next steps

The timeline for the RESTART project in the last months of this project is here commented with colours (green: done; yellow: delayed; red: overdue/not started):

Time	Activity	Implementation
December 2021	←Production of a full cell series for Rh inkjetting (~100 pcs.)	Hexis
January 2022	← Rh impregnation, Calcination and applying current collector layer ← Planning of the next series of button cell samples with input ZHAW	iPrint, Hexis ZHAW, Hexis Hexis, UMTEC

	← Conductivity Measurements of titanate materials (WP3) and Evaluation (ongoing)	
February 2022	← Stacking cells for system testing ← Start system testing ← Preparation of BC series	Hexis Hexis Hexis
March 2022	← BC Measurements ← Application for Innosuisse project (Inkjet Process development with iPrint)	Hexis iPrint, Hexis
April 2022	← EIS evaluation and postmortem microstructure analysis ← Optimized compositions for titanate materials; powder synthesis (not started) ← Paste preparation, measurement of in-plane conductivities (not started)	ZHAW UMTEC Hexis
May 2022	← Results from USTAN (Catalyst materials and their distribution, SOEC functionality)	Hexis (USTAN)
June 2022	← Alternative titanate compositions found to be tested on Shortstack and system level; powder synthesis and shipment to Hexis (not started)	UMTEC
July 2022	← Decision on preliminary cell design on prototype level (not started) ← Paste and cell preparation for Shortstack and system tests (not started)	Hexis, ZHAW, UMTEC Hexis
August 2022	← Catalyst Impregnation	iPrint
September 2022	← V1 Prototype Inkjet System established at iPrint, starting small series production (not started) ← Start Shortstack and System test on prototype level (not started)	iPrint (Innosuisse-Project) Hexis
October 2022		
November 2022	← Finalizing Evaluations, Thesis, Reports	Hexis, ZHAW, UMTEC
December 2022	← Issue all invoices	SFOE
January 2023	← Final Report (draft) submitted ← Financial Report (draft) submitted	Hexis, ZHAW, UMTEC
February 2023	check for completeness of all entries, feedback to project leader	SFOE

6 References

[1] X. Zhou, N. Yan, K. T. Chuang, and J. Luo, “Progress in La-doped SrTiO3 (LST)-based anode materials for solid oxide fuel cells,” RSC Adv., vol. 4, no. 1, pp. 118–131, 2014, doi: 10.1039/c3ra42666a.

[2] L. Shu, J. Sunarso, S. S. Hashim, J. Mao, W. Zhou, and F. Liang, “Advanced perovskite anodes for solid oxide fuel cells: A review,” Int. J. Hydrogen Energy, vol. 44, no. 59, pp. 31275–31304, 2019, doi: 10.1016/j.ijhydene.2019.09.220.

[3] A. Sciazko, Y. Komatsu, R. Yokoi, T. Shimura, and N. Shikazono, “Effects of mass fraction of La0.9Sr0.1Cr0.5Mn0.5O3-δ and Gd0.1Ce0.9O2-δ composite anodes for nickel free solid oxide fuel cells,” J. Eur. Ceram. Soc., vol. 42, no. 4, pp. 1556–1567, 2022, doi: 10.1016/j.jeurceram-soc.2021.11.039.

[4] D. Burnat, G. Nasdaurk, L. Holzer, M. Kopecki, and A. Heel, “Lanthanum doped strontium titanate - ceria anodes: deconvolution of impedance spectra and relationship with composition and microstructure,” J. Power Sources, vol. 385, no. February, pp. 62–75, 2018, doi: 10.1016/j.jpow-sour.2018.03.024.

[5] M. C. Verbraeken et al., “Short stack and full system test using a ceramic A-site deficient strontium titanate anode,” Fuel Cells, vol. 15, no. 5, pp. 682–688, 2015, doi: 10.1002/fuce.201400183.

[6] S. Primdahl and Y. L. Liu, “Ni Catalyst for Hydrogen Conversion in Gadolinia-Doped Ceria Anodes for Solid Oxide Fuel Cells,” J. Electrochem. Soc., vol. 149, no. 11, p. A1466, 2002, doi: 10.1149/1.1514234.

[7] C. D. Savaniu and J. T. S. Irvine, “La-doped SrTiO3 as anode material for IT-SOFC,” Solid State Ionics, vol. 192, no. 1, pp. 491–493, 2011, doi: 10.1016/j.ssi.2010.02.010.

[8] M. C. Verbraeken, B. Iwanschitz, A. Mai, and J. T. S. Irvine, “Evaluation of Ca Doped La 0.2 Sr 0.7 TiO 3 as an Alternative Material for Use in SOFC Anodes,” J. Electrochem. Soc., 2012, doi: 10.1149/2.001212jes.

[9] T. Ramos, S. Veltzé, B. R. Sudireddy, P. S. Jørgensen, L. Theil Kuhn, and P. Holtappels, “Effect of Ru/CGO versus Ni/CGO co-infiltration on the performance and stability of STN-based SOFCs,” Fuel Cells, vol. 14, no. 6, pp. 1062–1065, 2014, doi: 10.1002/fuce.201400013.

[10] R. Price, M. Cassidy, J. G. Grolig, A. Mai, and J. T. S. Irvine, “Preparation and Testing of Metal/Ce 0.80 Gd 0.20 O 1.90 (Metal: Ni, Pd, Pt, Rh, Ru) Co-Impregnated La 0.20 Sr 0.25 Ca 0.45 TiO 3 Anode Microstructures for Solid Oxide Fuel Cells,” J. Electrochem. Soc., vol. 166, no. 4, pp. F343–F349, 2019, doi: 10.1149/2.1181904jes.

[11] K. Bin Yoo and G. M. Choi, “LST-GDC composite anode on LaGaO3-based solid oxide fuel cell,” Solid State Ionics, vol. 192, no. 1, pp. 515–518, 2011, doi: 10.1016/j.ssi.2010.06.048.

[12] S. Futamura et al., “Alternative Ni-Impregnated Mixed Ionic-Electronic Conducting Anode for SOFC Operation at High Fuel Utilization,” J. Electrochem. Soc., vol. 164, no. 10, pp. F3055–F3063, 2017, doi: 10.1149/2.0071710jes.

[13] S. Futamura et al., “SOFC anodes impregnated with noble metal catalyst nanoparticles for high fuel utilization,” Int. J. Hydrogen Energy, vol. 44, no. 16, pp. 8502–8518, 2019, doi: 10.1016/j.ijhydene.2019.01.223.

[14] C. Graves, L. Martinez, and B. R. Sudireddy, “(Invited) High Performance Nano-Ceria Electrodes for Solid Oxide Cells,” ECS Trans., 2016, doi: 10.1149/07207.0183ecst.

[15] A. Nenning, M. Holzmann, J. Fleig, and A. K. Opitz, “Excellent kinetics of single-phase Gd-doped ceria fuel electrodes in solid oxide cells,” Mater. Adv., vol. 2, no. 16, pp. 5422–5431, 2021, doi: 10.1039/d1ma00202c.

[16] P. Blennow, K. Kammer Hansen, L. R. Wallenberg, and M. Mogensen, “Strontium Titanate-based Composite Anodes for Solid Oxide Fuel Cells,” ECS Trans., 2008, doi: 10.1149/1.3050390.

[17] C. Périllat-Merceroz, G. Gauthier, P. Roussel, M. Huvé, P. Gélin, and R. N. Vannier, “Synthesis and study of a Ce-doped La/Sr titanate for solid oxide fuel cell anode operating directly on methane,” Chem. Mater., vol. 23, no. 6, pp. 1539–1550, 2011, doi: 10.1021/cm103316b.

[18] N. Muzaffar, N. Arshad, D. B. Drasbæk, B. R. Sudireddy, and P. Holtappels, “Fabrication and electrochemical performance of zn-doped La 0.2 Sr 0.25 Ca 0.45 TiO 3 infiltrated with nickel-CGO, iron, and cobalt as an alternative anode material for solid oxide fuel cells,” Catalysts, vol. 9, no. 3, 2019, doi: 10.3390/catal9030269.

[19] C. Arrivé, T. Delahaye, O. Joubert, and G. Gauthier, “Exsolution of nickel nanoparticles at the surface of a conducting titanate as potential hydrogen electrode material for solid oxide electrochemical cells,” J. Power Sources, vol. 223, pp. 341–348, 2013, doi: 10.1016/j.jpowsour.2012.09.062.

[20] T. Zhu, H. E. Troiani, L. V. Mogni, M. Han, and S. A. Barnett, “Ni-Substituted Sr(Ti,Fe)O3 SOFC Anodes: Achieving High Performance via Metal Alloy Nanoparticle Exsolution,” Joule, vol. 2, no. 3, pp. 478–496, 2018, doi: 10.1016/j.joule.2018.02.006.

[21] A. M. Hussain, J. V. T. Hogh, W. Zhang, and N. Bonanos, “Efficient ceramic anodes infiltrated with binary and ternary electrocatalysts for SOFCs operating at low temperatures,” J. Power Sources, vol. 216, pp. 308–313, 2012, doi: 10.1016/j.jpowsour.2012.05.036.

[22] X. Li, H. Zhao, F. Gao, Z. Zhu, N. Chen, and W. Shen, “Synthesis and electrical properties of Co-doped Y0.08Sr0.92TiO3 - δ as a potential SOFC anode,” Solid State Ionics, vol. 179, no. 27–32, pp. 1588–1592, 2008, doi: 10.1016/j.ssi.2007.12.097.

[23] X. Sun, S. Wang, Z. Wang, X. Ye, T. Wen, and F. Huang, “Anode performance of LST-xCeO2 for solid oxide fuel cells,” J. Power Sources, vol. 183, no. 1, pp. 114–117, 2008, doi: 10.1016/j.jpowsour.2008.05.007.